
Fast Sampling for Flows and Diffusions with Lazy and Point Mass Stochastic Interpolants

Gabriel Damsholt¹ Jes Frellsen² Susanne Ditlevsen¹

Abstract

Stochastic interpolants unify flows and diffusions, popular generative modeling frameworks. A primary hyperparameter in these methods is the *interpolation schedule* that determines how to bridge a standard Gaussian base measure to an arbitrary target measure. We prove how to convert a sample path of a stochastic differential equation (SDE) with arbitrary diffusion coefficient under any schedule into the unique sample path under another arbitrary schedule and diffusion coefficient. We then extend the stochastic interpolant framework to admit a larger class of *point mass schedules* in which the Gaussian base measure collapses to a point mass measure. Under the assumption of Gaussian data, we identify *lazy* schedule families that make the drift identically zero and show that with deterministic sampling one gets a variance-preserving schedule commonly used in diffusion models, whereas with statistically optimal SDE sampling one gets our point mass schedule. Finally, to demonstrate the usefulness of our theoretical results on realistic highly non-Gaussian data, we apply our lazy schedule conversion to a state-of-the-art pretrained flow model and show that this allows for generating images in fewer steps without retraining the model.

1. Background

A basic goal of generative AI is to sample from a non-trivial target distribution, potentially in a very high-dimensional space, accessible only through a finite dataset of samples. Specifically, let $X^{(1)}, X^{(2)}, \dots, X^{(N)} \in \mathbb{R}^d$ be i.i.d. samples from an unknown distribution with density ρ_X . We then wish to generate new samples $X \sim \rho_X$.

¹Department of Mathematical Sciences, University of Copenhagen, Copenhagen, Denmark ²Department of Machine Learning and Signal Processing, Technical University of Denmark, Lyngby, Denmark. Correspondence to: Gabriel Damsholt <gnd@math.ku.dk>.

Preprint. February 4, 2026.

Various techniques for solving this basic generative problem exist. Many modern methods are based on *dynamical systems*. The idea is to learn the dynamics of a dynamical system with an analytically samplable initial law, typically taken to be standard Gaussian, and with final law ρ_X . Samples from ρ_X can then be generated by sampling from a standard Gaussian and integrating the dynamics from the initial to the final time.

We will use the flexible framework of *stochastic interpolants* (Albergo et al., 2025) which unifies flow and diffusion based generative models. We briefly introduce this framework and then state our contributions.

1.1. Spatially linear stochastic interpolant

The stochastic interpolant framework allows one to couple arbitrary distributions, and even arbitrarily many of them (Albergo et al., 2024), possibly in spatially non-linear ways and even using matrix coefficients (Negrel et al., 2025). We will exclusively work with the simplest and most commonly encountered setting, namely the “spatially linear one-sided stochastic interpolant” (Albergo et al., 2025, eq. 4.15) which we denote *stochastic interpolant* or just *interpolant*. Below we recall its definition and some core results.

Definition 1.1 (stochastic interpolant). Given independent random variables $Z, X \in \mathbb{R}^d$ with $Z \sim \mathcal{N}(0, \mathbf{I})$, $X \sim \rho_X$ and non-negative scalar functions $\alpha, \beta : [0, 1] \rightarrow [0, \infty)$ satisfying the below criteria, the *stochastic interpolant* or simply *interpolant* is the stochastic process

$$I_t = \alpha_t Z + \beta_t X, \quad t \in [0, 1],$$

with $\alpha, \beta \in C^1([0, 1])$ satisfying the boundary conditions $\alpha_0 = \beta_1 = 1$, $\alpha_1 = \beta_0 = 0$ and the monotonicity conditions $\dot{\alpha}_t < 0$ and $\dot{\beta}_t > 0$ for all $t \in (0, 1)$.¹

Note that $I_0 \sim \mathcal{N}(0, \mathbf{I})$ and $I_1 \sim \rho_X$ for all valid choices of α, β .

One of the primary objects of interest is the following.

¹One can allow for the one-sided derivatives of α and β to explode at either endpoint as long as the one-sided derivatives exist in the extended reals, see Albergo et al. (2025) for a discussion on this. We require bounded derivatives for simplicity.

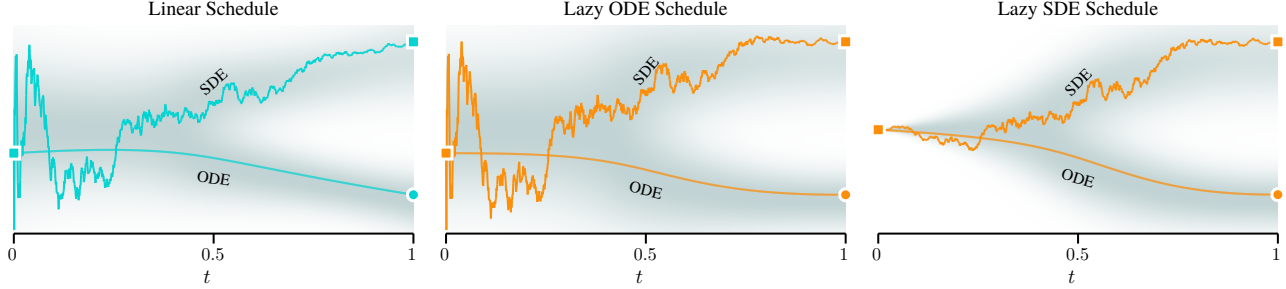


Figure 1. ODE ($\varepsilon \equiv 0$) and statistically optimal SDE ($\varepsilon = \varepsilon^*$) sample path under three different interpolation schedules for ρ_X a Gaussian mixture density for which the dynamics are analytically known (Albergo et al., 2025, Appendix A). All paths start in the same initial condition which sits in the initial position (cyan circle) for the leftmost two interpolants with density-admitting schedule and in the initial drift for the rightmost point mass schedule. The same Wiener process realization is shared between all three SDE solutions. Leftmost is the linear schedule from Definition 5.1, middle and rightmost is the lazy interpolant for the ODE and statistically optimal SDE, respectively, as in Example 7.4. Since $u_t = t$ for all three schedules, all sample paths are equivalent up to a reparameterization of space. Note that all sample paths end in the same position for the ODE and SDE, respectively. See Figure 4 for a plot of the three schedules and their statistically optimal diffusion scales.

Definition 1.2 (schedule). The function pair (α, β) in Definition 1.1 is the *interpolation schedule* or simply *schedule*.

The schedule is a hyperparameter that determines how $\mathcal{N}(0, \mathbf{I})$ and ρ_X are bridged in time. A canonical choice is $\alpha_t = 1 - t$, $\beta_t = t$; this is the choice taken in flow matching.

To proceed we define the following functions.

Definition 1.3. For an interpolant as in Definition 1.1 with density $\rho : [0, 1] \times \mathbb{R}^d \rightarrow (0, \infty)$ and $\varepsilon : [0, 1] \rightarrow [0, \infty)$ we define the following functions for $(t, x) \in [0, 1] \times \mathbb{R}^d$:

$$\begin{aligned} \eta_Z(t, x) &:= \mathbb{E}[Z \mid I_t = x], & \text{“noise predictor”} \\ \eta_X(t, x) &:= \mathbb{E}[X \mid I_t = x], & \text{“data predictor”} \\ s(t, x) &:= \nabla \log \rho(t, x), & \text{“score”} \\ b^\varepsilon(t, x) &:= \dot{\alpha}_t \eta_Z(t, x) + \dot{\beta}_t \eta_X(t, x) + \varepsilon_t s(t, x). & \text{“drift”} \end{aligned}$$

The central idea behind the stochastic interpolant framework is to construct a family of *stochastic differential equations* (SDEs) indexed by an arbitrary time-dependent additive diffusion scale $\varepsilon : [0, 1] \rightarrow [0, \infty)$, whose solutions have the same marginal distributions (but different joint distributions) as I_t , as captured in the following theorem (Albergo et al., 2025, Corollary 18).

Theorem 1.4 (SDE). *Let $\varepsilon_t \in C^1([0, 1])$ be any non-negative scalar function. Then the solutions to the SDE*

$$dX_t^\varepsilon = b^\varepsilon(t, X_t^\varepsilon) dt + \sqrt{2\varepsilon_t} dW_t, \quad (1)$$

solved forward in time t with $X_0^\varepsilon \sim \mathcal{N}(0, \mathbf{I})$ independent of W , satisfy $\text{Law}(X_t^\varepsilon) = \text{Law}(I_t)$ for all $t \in [0, 1]$.

With the above result we can pick any non-negative diffusion scale ε , sample $X_0^\varepsilon \sim \mathcal{N}(0, \mathbf{I})$ and solve the SDE forward in time from $t = 0$ to $t = 1$ provided we know the drift b^ε . Then $X_1^\varepsilon \sim \rho_X$, as desired. In particular, setting $\varepsilon \equiv 0$ gives a deterministic probability flow ODE.

Each function in Definition 1.3 can be characterized as the minimizer of a simple squared-loss objective, enabling unbiased Monte-Carlo estimation from data without simulating the SDE. One then uses the learned estimate of the dynamics to generate data, e.g. one learns $\hat{b}^\varepsilon \approx b^\varepsilon$ from data and solves the SDE (1) with b^ε replaced by \hat{b}^ε to sample $\hat{X} \sim \hat{\rho}_X \approx \rho_X$.

Throughout we assume the following, the validity of which depends on the properties of ρ_X , the smoothness of (α, β) and the choice of ε (see Albergo et al. (2025) for details).

Assumption 1.5. The data density satisfies $\rho_X(x) > 0$ for all $x \in \mathbb{R}^d$, and the density $\rho : [0, 1] \times \mathbb{R}^d \rightarrow (0, \infty)$ of the interpolant satisfies $\rho(\cdot, x) \in C^1([0, 1])$ for all $x \in \mathbb{R}^d$, $\rho(t, \cdot) \in C^2(\mathbb{R}^d)$ for all $t \in [0, 1]$, and similarly for the functions in Definition 1.3. Furthermore, the SDE (1) has a unique strong solution for all initial conditions.

2. Contributions

1. In Theorem 5.5 we generalize existing results from the ODE to the SDE setting and show that we can uniquely convert any strong solution to the SDE (1) with arbitrary schedule and diffusion scale into the corresponding strong solution to the SDE (1) with an arbitrary different schedule and diffusion scale.
2. In Definition 6.1 and Theorem 6.3 we extend the interpolation schedule to include the point mass boundary condition $\alpha_0 = 0$ and give sufficient conditions for the SDE to exist in this extended setting with normally distributed initial conditions that sit in the initial drift instead of in the initial position. We stress that this result even holds in the ODE case, i.e. when $\varepsilon \equiv 0$.
3. Assuming that $X \sim \mathcal{N}(0, \mathbf{I})$ we prove in Proposition 7.1 that the *lazy schedule family* – the family of schedules such that the dynamics become identically zero – for

the ODE satisfies the variance-preserving property $\alpha_t^2 + \beta_t^2 = 1$, while for the SDE with statistically optimal diffusion scale it satisfies $\alpha_t^2 + \beta_t^2 = \beta_t$. In particular, $\alpha_0 = 0$ in the latter case, which motivates our schedule extension to the point mass case.

4. In Propositions 7.5 and 7.6 and Algorithms 1 and 2 we derive particularly simple and theoretically well-motivated formulas for reparameterizing space (but not time) in any pretrained flow matching model with linear schedule $\bar{\alpha}_t = 1 - t$, $\bar{\beta}_t = t$ to yield a lazy ODE and statistically optimal SDE schedule, respectively.
5. In Section 8 we conduct empirical experiments with a state-of-the-art flow matching model for natural image generation and show that using this reparameterization allows for fewer-step numerical sampling in the ODE case and especially so for the statistically optimal SDE, which is otherwise numerically undefined at $t = 0$.

3. Related work

The stochastic interpolant framework (Albergo et al., 2025) unifies existing continuous-time generative paradigms based on dynamical systems, namely flow matching (Lipman et al., 2023) and diffusion models² (Sohl-Dickstein et al., 2015; Song & Ermon, 2019; Song et al., 2021) by disentangling the two primary hyperparameters: the *interpolation schedule* coupling the Gaussian and data distribution in time, and the *stochasticity* of the stochastic process that samples this coupling. The optimal level of stochasticity has mostly been explored in the stochastic interpolant literature (Albergo et al., 2025; Chen et al., 2024; Ma et al., 2024; Chen et al., 2025), whereas more work exists on tuning the interpolation schedule with the aim of easing numerical integration, albeit often heuristically or empirically based (Nichol & Dhariwal, 2021; Karras et al., 2022; Song & Ermon, 2020; Xue et al., 2024). Our work is primarily inspired by Chen et al. (2025), but by considering the statistically optimal SDE instead of just the ODE we arrive at *point mass schedules* for which little work exists (Albergo et al., 2025; Chen et al., 2024). Our work also resembles Sabour et al. (2024), but in addition to time reparameterizations we also consider space reparameterizations, even extending to point mass schedules.

Changing the interpolation schedule post-training has recently been explored for ODE sampling (Liu, 2024; Lai et al., 2025; Chen et al., 2025), but to the best of our knowledge pathwise equivalence has never been established for SDE sampling before.

More sophisticated approaches for sampling from flow and diffusion models in fewer steps exist; some notable exam-

²Score-based generative models, the continuous-time equivalents of denoising diffusion probabilistic models (Ho et al., 2020).

ples are flow rectification (Liu et al., 2023), consistency models (Song et al., 2023; Boffi et al., 2025) and (entropy regularized) optimal transport based approaches (Pooladian et al., 2023; Shi et al., 2023; Bortoli et al., 2021; Pooladian & Niles-Weed, 2025). These approaches are mostly supplementary to the choice of schedule that we explore.

4. Intra-interpolant conversion formulas

In this section we fix the schedule (α, β) and show how to convert between the functions in Definition 1.3. The proofs can be found in Appendix A.

The following diffusion scale plays an important role in our work. We define it now and motivate it later.

Definition 4.1. Given an interpolation schedule (α, β) satisfying the criteria in Definition 1.1 we denote by $\varepsilon_t^* : [0, 1] \rightarrow [0, \infty]$ the scalar function

$$\varepsilon_t^* = \alpha_t^2 \frac{\dot{\beta}_t}{\beta_t} - \alpha_t \dot{\alpha}_t,$$

where at $t = 0$ the equation is interpreted as a right-limit in the extended reals.

We start by showing that for a fixed interpolation schedule (α, β) , any one of the functions from Definition 1.3 uniquely defines all remaining functions through affine transformations that simplify using the above definition for ε^* . This result generalizes the well-known result relating the score to the noise predictor (Albergo et al., 2025, Theorem 8) and Lai et al. (2025, Proposition 6.3.1) for the ODE case $\varepsilon \equiv 0$.

Proposition 4.2 (intra-interpolant conversion formulas). *For a fixed interpolation schedule (α, β) and non-negative $\varepsilon \in C^1([0, 1])$, each of the functions $\eta_Z, \eta_X, s, b^\varepsilon$ uniquely defines all of the others on $(0, 1) \times \mathbb{R}^d$. In particular, each function can be expressed in terms of the score as*

$$\begin{aligned} \eta_Z(t, x) &= -\alpha_t s(t, x), \\ \eta_X(t, x) &= (x + \alpha_t^2 s(t, x)) / \beta_t, \\ b^\varepsilon(t, x) &= (\varepsilon_t^* + \varepsilon_t) s(t, x) + (\dot{\beta}_t / \beta_t) x. \end{aligned}$$

The next theorem characterizes ε^* as the statistically optimal diffusion scale in a precise sense. This is essentially equation 13 in Chen et al. (2024) but our proof is simpler.

Theorem 4.3. *Assume we are given statistically learnt estimates $\hat{\eta}_Z, \hat{\eta}_X, \hat{s}$ or \hat{b}^ε of the true functions from Definition 1.3 with remaining estimates given by Proposition 4.2. Let X_t^ε solve the SDE (1) and consider the plug-in SDE*

$$d\hat{X}_t^\varepsilon = \hat{b}^\varepsilon(t, \hat{X}_t^\varepsilon) dt + \sqrt{2\varepsilon_t} dW_t,$$

solved forward in time t with $\hat{X}_0^\varepsilon \sim \mathcal{N}(0, \mathbf{I})$ independent of W . Then the minimizer of the Kullback-Leibler divergence

between the path measures of X^ε and \hat{X}^ε over the diffusion scale ε is

$$\operatorname{argmin}_{\varepsilon \geq 0, \varepsilon \in C^1((0,1])} \operatorname{KL}\left(X^\varepsilon, \hat{X}^\varepsilon\right) = \varepsilon^*,$$

and the minimum is

$$\operatorname{KL}\left(X^{\varepsilon^*}, \hat{X}^{\varepsilon^*}\right) = \int_0^1 \varepsilon_t^* \mathbb{E}\left[\|s(t, I_t) - \hat{s}(t, I_t)\|^2\right] dt.$$

Unfortunately, the statistically optimal diffusion scale ε^* is ill-behaved numerically in the sense that for any schedule (α, β) satisfying Definition 1.1 it is infinite and non-integrable at $t = 0$ (Proposition B.1). Nonetheless, the *statistically optimal SDE*, i.e., the SDE (1) with $\varepsilon = \varepsilon^*$, is well-defined on $t \in (0, 1]$ and behaves like a (non-continuous) white-noise process as $t \rightarrow 0_+$. See Proposition B.5 which proves an equivalence between ε^* , the Ornstein-Uhlenbeck process, and diffusion models.

5. Inter-interpolant conversion formulas

We now show how to convert the functions from Definition 1.3 from one schedule to another and how to convert between solutions to the SDEs. The following *linear schedule* used in flow matching simplifies the conversion formulas.

Definition 5.1 (linear interpolant). Let $\bar{\alpha}_t := 1 - t$, $\bar{\beta}_t := t$. Then we denote by $\bar{I}_t := \bar{\alpha}_t Z + \bar{\beta}_t X$ the *linear interpolant*. We denote by $\bar{\eta}_Z, \bar{\eta}_X, \bar{s}, \bar{b}^{\bar{\varepsilon}}$ its associated functions as in Definition 1.3 and by $\bar{X}_t^{\bar{\varepsilon}}$ its associated SDE (1).

Proposition 5.2. For the linear interpolant \bar{I}_t from Definition 5.1 it holds that $\bar{\varepsilon}_t^* = (1 - t)/t$. Therefore

$$\int_s^t 2\bar{\varepsilon}_u^* du = 2(\log(t) - t - \log(s) + s)$$

for $0 < s \leq t \leq 1$ and the integral is infinite for $s = 0$.

Definition 5.3. For $t \in [0, 1]$ we define the functions

$$c_t := \alpha_t + \beta_t, \quad u_t := \beta_t/c_t.$$

The interpretation is that c is a (generally non-invertible) space-change while u is a proper time change. Indeed, the monotonicity assumptions on the schedule (α, β) in Definition 1.1 imply that $u \in C^1([0, 1])$ and is strictly increasing on $(0, 1)$ so that its inverse $t_u := u^{-1}(u)$ exists.

The following proposition can be seen as a supplement to Proposition 4.2. It rephrases and generalizes proposition 3.1 from Chen et al. (2025) and proposition 6.3.3 from Lai et al. (2025) which only consider the ODE case ($\varepsilon \equiv 0$).

Proposition 5.4 (inter-conversion formulas). For a schedule (α, β) and non-negative $\varepsilon \in C^1([0, 1])$, the functions

$\eta_Z, \eta_X, s, b^\varepsilon$ are uniquely defined from any of the functions $\bar{\eta}_Z, \bar{\eta}_X, \bar{s}, \bar{b}^{\bar{\varepsilon}}$ associated with the linear interpolant. In particular,

$$\begin{aligned} \eta_Z(t, x) &= \bar{\eta}_Z(u_t, x/c_t), & \eta_X(t, x) &= \bar{\eta}_X(u_t, x/c_t), \\ s(t, x) &= (1/c_t)\bar{s}(u_t, x/c_t), \\ b^\varepsilon(t, x) &= \frac{\dot{c}_t}{c_t}x + c_t \dot{u}_t \bar{b}^{\bar{\varepsilon}}\left(u_t, \frac{x}{c_t}\right) \quad \text{for } \bar{\varepsilon}_{u_t} = \frac{\alpha_t \varepsilon_t}{\beta_t \varepsilon_t^*}. \end{aligned}$$

We finally prove our strongest conversion result, which to the best of our knowledge is new for $\varepsilon \not\equiv 0$.

Theorem 5.5 (pathwise conversion). Let (α, β) be a schedule satisfying the requirements in Definition 1.1, let $z \in \mathbb{R}^d$ and let $(W_t)_{t \in [0, 1]}$ be a Wiener process realization. Let X_t^ε solve the SDE (1) in physical time t from $X_0^\varepsilon = z$ driven by W with diffusion scale ε . Let $\bar{X}_u^{\bar{\varepsilon}}$ solve the SDE (1) with linear schedule in reparameterized time $u = u_t$ from $\bar{X}_0^{\bar{\varepsilon}} = z$ driven by

$$\bar{W}_u = \int_0^{t_u} \sqrt{\dot{u}_s} dW_s, \quad u \in [0, 1]$$

with diffusion scale $\bar{\varepsilon}_u = (\alpha_{t_u} \varepsilon_{t_u})/(\beta_{t_u} \varepsilon_{t_u}^*)$. Then the solution X_t^ε can be obtained from the solution $\bar{X}_{u_t}^{\bar{\varepsilon}}$ associated with the linear interpolant via the formula

$$X_t^\varepsilon = c_t \bar{X}_{u_t}^{\bar{\varepsilon}}, \quad t \in [0, 1].$$

In particular, $X_1^\varepsilon = \bar{X}_1^{\bar{\varepsilon}}$ (since $c_1 = 1$).

With this result, we can sample paths from the interpolant with any schedule and any diffusion scale provided we can sample paths from the linear interpolant (simply apply Theorem 5.5 twice to convert from an arbitrary schedule instead of the linear schedule). This is illustrated in the two leftmost plots in Figure 1 for the ODE and statistically optimal SDE, respectively.

Remark 5.6. We shall see that the identity time-transform $u_t = t$ is of particular interest. Then Theorem 5.5 simplifies significantly, in particular, $\bar{W} = W$.

6. Point mass schedule

We use the preceding results to extend Definition 1.1 to transport to the target distribution from a point mass instead of a (non-degenerate) Gaussian. We delay the motivation to the next section.

Definition 6.1 (point mass schedule and interpolant). A function pair $\alpha, \beta \in C^1([0, 1])$ satisfying

1. $\alpha_0 = \alpha_1 = \beta_0 = 0, \beta_1 = 1$,
2. $\alpha_t > 0, \dot{\beta}_t > 0$ for all $t \in (0, 1)$,

3. $\beta_t = o(\alpha_t)$ as $t \rightarrow 0_+$ (equivalently $u_0 = 0$),
4. $\alpha_t^2 = O(\beta_t)$ as $t \rightarrow 0_+$,
5. $\dot{u}_0 := \lim_{t \rightarrow 0_+} \dot{u}_t < \infty$,
6. $\frac{d}{dt}(\beta_t/\alpha_t) > 0$ for all $t \in (0, 1)$ (equivalently $\dot{u}_t > 0$),

we call a *point mass schedule*. The associated interpolant we call a *point mass interpolant*.

Remark 6.2. The condition $\alpha_0 = \beta_0 = 0$ is sufficient and necessary for the density of the interpolant to collapse to a point mass at $t = 0$. The condition $u_0 = 0$ is sufficient and necessary for the initial drift to be analytically samplable; if otherwise $u_0 > 0$ we would have to sample the non-trivial law of $\bar{I}_{u_0} \neq \bar{I}_0$ to sample the initial drift, which is impossible in practice. The condition $\alpha_t^2 = O(\beta_t)$ as $t \rightarrow 0_+$ is technical and can be relaxed; see the remarks at the end of the proof of Theorem 6.3. The assumption $\dot{u}_0 < \infty$ gives $u \in C^1([0, 1])$, which is not strictly necessary but we impose it for simplicity. The last assumption is equivalent to $\dot{u}_t > 0$ for all $t \in (0, 1)$ so that $t \mapsto u_t$ is a proper time change.

Remarkably, the initial drift of the point mass interpolant can be defined pointwise from the initial condition of the linear interpolant, even in the ODE case, as we show below.

Theorem 6.3. *Let (α, β) be a point mass schedule as in Definition 6.1. Then given any non-negative bounded diffusion scale $\varepsilon \in C^1([0, 1])$, the SDE (1) is well-defined in the classical sense for $t \in (0, 1]$ with initial position $X_0^\varepsilon = 0$, and the initial drift is well-defined in distribution. It holds that $\text{Law}(X_t^\varepsilon) = \text{Law}(I_t)$ for all $t \in [0, 1]$ and Theorem 5.5 still applies: in particular, the point mass SDE solution and initial drift relates to the solution and initial condition of the linear interpolant as $X_t^\varepsilon = c_t \bar{X}_{u_t}^\varepsilon$ for $t \in [0, 1]$ and $b^\varepsilon(0, X_0^\varepsilon) = (\dot{c}_0 - \lim_{t \rightarrow 0_+} (\varepsilon_t/\alpha_t)) \bar{X}_0^\varepsilon$.*

Remark 6.4. The initial drift in Theorem 6.3 is always bounded for the ODE case $\varepsilon \equiv 0$, whereas for the SDE case it is bounded if and only if we choose the diffusion scale such that $\varepsilon_t \in O(\alpha_t)$ as $t \rightarrow 0_+$.

Theorem 6.3 shows that while the normally distributed initial condition sits at the initial position for the density-admitting stochastic interpolant from Definition 1.1, the initial condition instead sits at the initial SDE drift (or ODE velocity when $\varepsilon \equiv 0$) for the point mass interpolant from Definition 6.1. To the best of our knowledge such a non-standard ODE has not been considered before in the flow or diffusion literature, whereas the SDE has been treated in slightly different settings in Albergo et al. (2025); Chen et al. (2024).

A sample path from a point mass interpolant is plotted together with its linear interpolant path in Figure 1 for the ODE and statistically optimal SDE, respectively.

We finally extend proposition 2.5 from Chen et al. (2025) to the point mass setting.

Proposition 6.5. *Let (α, β) be any valid schedule, possibly a point mass schedule. Then under the assumptions in Theorem 4.3, the minimal path-measure KL-divergence attained when $\varepsilon = \varepsilon^*$ is invariant to the choice of schedule.*

Proposition 6.5 dictates that we must optimize the schedule for some criterion different from statistical optimality, which is what we do in the next section.

7. Lazy schedules under Gaussian data assumption

In this section, we make the oversimplifying assumption that $X \sim \mathcal{N}(0, \mathbf{I})$. This allows us to identify families of schedules for which the SDE drift is identically zero, the motivation being that such schedules minimize the energy required to transport from base to target measure. We call these schedules *lazy*. In the experimental section, we demonstrate empirically that the results we obtain under the Gaussian data assumption are useful even in realistic, high-dimensional and highly non-Gaussian settings.

7.1. Relation to flows and diffusions

To simplify the presentation we focus on two natural choices for the diffusion scale: $\varepsilon \equiv 0$ and $\varepsilon = \varepsilon^*$. The former corresponds to ODE sampling and reduces to standard flow matching under the linear interpolant (see Definition 5.1). The latter reduces to sampling a time-reversed Ornstein-Uhlenbeck process as in diffusion modeling (Proposition B.5) and we will henceforth refer to this as “statistically optimal SDE sampling”. Numerical integration is simpler for ODE sampling, but statistically optimal SDE sampling is maximally robust to approximation errors in the learned drift estimate as per Theorem 4.3. Throughout we use the notation $b := b^{\varepsilon \equiv 0}$ for the ODE velocity and $b^* := b^{\varepsilon = \varepsilon^*}$ for the statistically optimal SDE drift.

7.2. Identifying lazy schedules

Requiring the velocity and drift to be identically zero under the Gaussian data assumption removes one degree of freedom in the schedule.

Proposition 7.1 (lazy schedule families). *Assume that $X \sim \mathcal{N}(0, \mathbf{I})$. Then for all $(t, x) \in [0, 1] \times \mathbb{R}^d$ it holds that*

1.

$$b(t, x) = 0 \iff \alpha_t^2 + \beta_t^2 = 1.$$

In words, the ODE velocity is identically zero if and only if the schedule is variance preserving.

2.

$$b^*(t, x) = 0 \iff \alpha_t^2 + \beta_t^2 = \beta_t.$$

This implies $\alpha_0 = 0$, $\beta_t = o(\alpha_t)$, $\alpha_t^2 = O(\beta_t)$ as $t \rightarrow 0_+$. We have that $i_0 < \infty \iff \dot{\beta}_t = O(\sqrt{\beta_t})$ in which case the schedule is a point mass schedule per Definition 6.1. It also holds for all $t \in [0, 1]$ that $\varepsilon_t^* = \dot{\beta}_t/2$ so that

$$\int_s^t 2\varepsilon_u^* du = \beta_t - \beta_s \quad \text{for } 0 \leq s \leq t \leq 1.$$

Proposition 7.1 curiously shows that requiring the ODE velocity to be identically zero under the Gaussian data assumption amounts to choosing a variance preserving schedule, which is typically used in diffusion models but not in flow models. On the other hand, for statistically optimal SDE sampling it instead leads to point mass schedule, which is underexplored in the literature.

Remark 7.2. From Proposition 7.1 together with the inevitable boundary conditions $\beta_0 = 0$, $\beta_1 = 1$ we see that $\int_0^1 2\varepsilon_u^* du = 1$, i.e. the quadratic variation of the martingale part of solutions to our SDE from $t = 0$ to $t = 1$ are fixed at 1. This is remarkable since for $\alpha_0 = 1$ the same integral is fixed at ∞ by Proposition B.1. This result holds even when X is not normally distributed. However, one easily shows that normalizing this quadratic variation by the total variance gives $\int_0^t (2\varepsilon_u^*)/\beta_u du = [\log(\beta_u)]_0^t = \infty$ for all $t \in (0, 1]$, resembling the result from Proposition B.1.

A natural next question is how to eliminate the last degree of freedom. We give two natural examples below and then discuss why the second example is useful in practice.

Example 7.3 ($\beta_t = t$). Setting $\beta_t = t$ gives, in the ODE case, $\alpha_t = \sqrt{1 - t^2}$. Interestingly, this is not the usual linear schedule used in flow matching models. Also $\dot{\alpha}_1 = -\infty$. Considering instead the SDE case we get $\alpha_t = \sqrt{t(1-t)}$ and $2\varepsilon_t^* = 1$. When $X \sim \mathcal{N}(0, \mathbf{I})$, the solution to the SDE is a standard d -dimensional Brownian motion $(W_t)_{t \in [0, 1]}$ with $W_0 = 0$. Also $\dot{\alpha}_0 = \infty$ and $\dot{\alpha}_1 = -\infty$. The endpoint explosion of $\dot{\alpha}$ in these schedules is worrisome.

Example 7.4 ($u_t = t$). Define $d_t := (1-t)^2 + t^2$. Then for the ODE case requiring $u_t = t$ gives the schedule $\alpha_t = (1-t)/\sqrt{d_t}$, $\beta_t = t/\sqrt{d_t}$. Then $\dot{\alpha}_0 = 0$, $\dot{\alpha}_1 = -1$ and $\dot{\beta}_0 = 1$, $\dot{\beta}_1 = 0$. Considering instead the SDE case gives the schedule $\alpha_t = t(1-t)/d_t$, $\beta_t = t^2/d_t$ which is a point mass schedule per Proposition 7.1 since $\dot{\beta}_t = O(\sqrt{\beta_t})$ as $t \rightarrow 0_+$. We now have $\dot{\alpha}_0 = 1$, $\dot{\alpha}_1 = -1$ and $\dot{\beta}_0 = \dot{\beta}_1 = \varepsilon_0^* = \varepsilon_1^* = 0$, and also $\dot{c}_0 = 1 = \lim_{t \rightarrow 0_+} \varepsilon_t^*/\alpha_t$ so that the initial drift is zero per Theorem 6.3. The fact that all functions are bounded everywhere in both schedules is attractive from a numerical perspective.

We can further characterize and motivate the constraint $u_t = t$ in Example 7.4 as follows. Consider the log-signal-to-noise ratio $\lambda_t := \log(\beta_t^2/\alpha_t^2)$. Thus, $\lambda_0 = -\infty$ and $\lambda_1 = \infty$.³ It might be natural to require λ_t to be linear

in *logit-time*. Specifically, define $\tau(t) := 2 \log(t/(1-t))$, with inverse $t(\tau) = (1 + \exp(-\tau/2))^{-1}$, i.e. the logistic function with growth rate 1/2. Then requiring $\lambda_t = \tau(t)$ is equivalent to requiring $u_t = t$.

7.3. Lazy schedule transformation of a pretrained flow matching model

Based on what we have shown so far, we can convert any flow or diffusion model (more generally any stochastic interpolant) with an arbitrary schedule to its corresponding lazy schedule variant (under the Gaussian assumption). The motivation is that numerically solving the ODE or SDE is easier when the dynamics are gentle. That the dynamics in practice become gentler under the lazy schedule even when we seriously violate the Gaussian data assumption is strongly suggested by the empirical results in the next section. To make the schedule conversion particularly simple, we focus on the $u_t = t$ case considered in Example 7.4. We focus on converting from a flow matching model velocity v^{flow} , which is identical to the linear ODE velocity \bar{b} of the linear interpolant \bar{I}_t from Definition 5.1 (see also Appendix B.1).

Proposition 7.5 (linear velocity to lazy ODE velocity). Define the schedule

$$\alpha_t := (1-t)/\sqrt{d_t}, \quad \beta_t := t/\sqrt{d_t}, \quad d_t := (1-t)^2 + t^2,$$

as in Example 7.4 and assume we are given access to the ODE velocity $\bar{b} = v^{\text{flow}}$ of the linear interpolant from Definition 5.1. Then the velocity satisfies

$$b(t, x) = ((1-2t)/(d_t))x + (1/\sqrt{d_t})\bar{b}(t, \sqrt{d_t}x),$$

for all $(t, x) \in [0, 1] \times \mathbb{R}^d$. In particular, the initial velocity satisfies

$$b(0, z) = z + \bar{b}(0, z) = \mathbb{E}[X] \quad \forall z \in \mathbb{R}^d.$$

Proposition 7.6 (linear velocity to lazy SDE drift). Define the schedule

$$\alpha_t := t(1-t)/d_t, \quad \beta_t := t^2/d_t, \quad d_t := (1-t)^2 + t^2,$$

as in Example 7.4 and assume we are given access to the ODE velocity $\bar{b} = v^{\text{flow}}$ of the linear interpolant from Definition 5.1. Then the statistically optimal SDE drift satisfies

$$b^*(t, x) = (2/d_t)((1-2t)x + t\bar{b}(t, (d_t/t)x)),$$

for all $(t, x) \in (0, 1] \times \mathbb{R}^d$, and the initial drift is identically zero, i.e. $b^*(0, 0) = 0$.

We can restate Propositions 7.5 and 7.6 as particularly simple algorithms for how to solve the lazy ODE and SDE using

³Even if the schedule is a point mass schedule we still have the

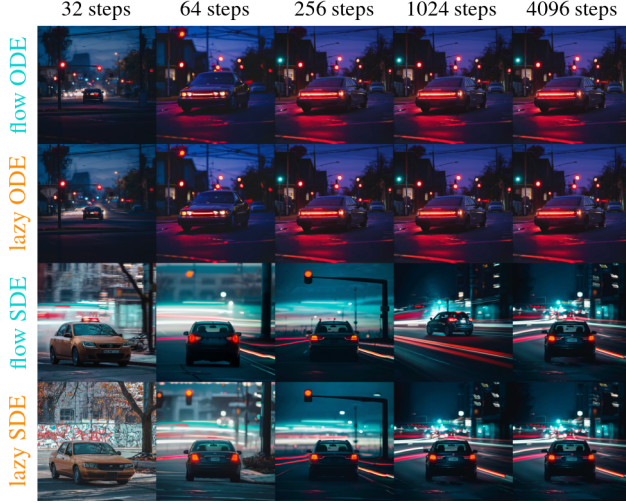


Figure 2. Sample images from the PRX flow model with a varying number of predictor-corrector steps for the ODE and statistically optimal SDE, respectively, sampled using the original linear `flow` model schedule versus converting to the `lazy` schedule. The text prompt “A car is stopped at a red light” was used. As expected, the image quality improves as the number of solver steps increases and seems to converge to the “ground truth” reference image which depends on whether an ODE or SDE is used but less so on which schedule is used. See [this Zenodo link](#) for an animation.

the linear ODE velocity. Pseudocode for these algorithms is given in Algorithms 1 and 2.

We stress that we can prove results similar to Propositions 7.5 and 7.6 but from a pretrained diffusion model instead of flow model, or more generally from a pretrained stochastic interpolant with any schedule and any training objective. This is omitted for brevity.

Remark 7.7. Note that Propositions 7.5 and 7.6 generally do not hold exactly when we only have access to an approximate linear flow velocity $\hat{v}^{\text{flow}} \approx v^{\text{flow}}$ learned from data, as is always the case in practice.

8. Experiments

To investigate the usefulness of our lazy schedules in realistic, high-dimensional settings with highly non-Gaussian data we conduct experiments on the latest, largest Phototroom Experimental (PRX) text-to-image classifier-free guided latent-space flow model (Phototroom, 2025; Almazán et al., 2025; Lipman et al., 2023; Ho & Salimans, 2022) which has around 1.3 billion parameters and is currently in beta⁴. We fix the guidance strength at the recommended value of 5 and wish to investigate whether dynamically converting to the lazy schedules using Propositions 7.5 and 7.6 as described in detail in Algorithms 1 and 2 enables us to generate good images in fewer steps using the ODE and

⁴ Available on HuggingFace at <https://huggingface.co/Phototroom/prx-1024-t2i-beta>.

statistically optimal SDE, respectively. We use the predictor-corrector scheme which informally is a mix between the explicit Euler(-Maruyama) scheme and the Heun scheme and which we find is the most efficient of the three. See Appendix E for a precise definition of each scheme and some sample image comparisons.

Instead of looking at standard but arbitrary goodness-of-image metrics such as Fréchet Inception distance (Heusel et al., 2017) and Inception score (Salimans et al., 2016), we look at how fast the predictor-corrector solver converges to the idealized “ground truth” reference image as a function of the total number of numerical solver steps n_i . Since the idealized “ground truth” reference image is unattainable in practice, we define it as the average image after $n_k = 4096 \approx \infty$ solver steps, i.e.,

$$\text{img}_{\text{reference}}^{\text{ODE}} := (\text{img}_{4096}^{\text{ODE,flow}} + \text{img}_{4096}^{\text{ODE,lazy}})/2,$$

and similarly for the SDE. This is reasonable since in the idealized setting where $\hat{v}^{\text{flow}} = v^{\text{flow}}$, i.e. when the flow velocity is learned perfectly, then $\text{img}_{\infty}^{\text{ODE,flow}} = \text{img}_{\infty}^{\text{ODE,lazy}}$, and similarly for the SDE. Results where $\text{img}_{\text{reference}}^{\text{ODE}} := \text{img}_{4096}^{\text{ODE,flow}}$ is used instead are shown in Figure 9.

As text prompts we use the first 100 captions from the COCO validation dataset (Lin et al., 2014; Chen et al., 2015) as listed in Appendix G. For each experiment we fix a text prompt from our dataset and randomly sample an initial condition and (for SDE generation) a Wiener process realization. We let the number of numerical solver steps vary in the range $n_1 = 4, n_2 = 8, \dots, n_k = 4096$. This generates $k = 11$ images of increasing quality for each of the four configurations (ODE, SDE) \times (`flow`, `lazy`) sharing the same prompt, initial condition and Wiener process realization, as illustrated in Figure 2. We then calculate the root mean square error (RMSE) over pixels⁵ between the image produced with n_i numerical solver steps and the reference image, i.e. we calculate

$$\text{RMSE}(\text{img}_{n_i}^{\text{ODE,flow}}, \text{img}_{\text{reference}}^{\text{ODE}})$$

for each i and similarly for $\text{img}_{n_i}^{\text{ODE,lazy}}$ and the SDE. We repeat this experiment for each of our 100 different prompts, initial conditions and Wiener process realizations and compute the average RMSE. This measures numerical convergence of the solver under each configuration.⁶ The result is plotted in Figure 3 and animations for the generated images for all 100 prompts are accessible at [this Zenodo link](#).

Under the linear flow model schedule the statistically optimal SDE has infinite initial drift and diffusion scale

⁵This corresponds to a dimension-normalized Euclidean distance in pixel-space.

⁶To be precise, this measures convergence of the latent representations *after* decoding, which is more semantically meaningful than convergence in latent space.

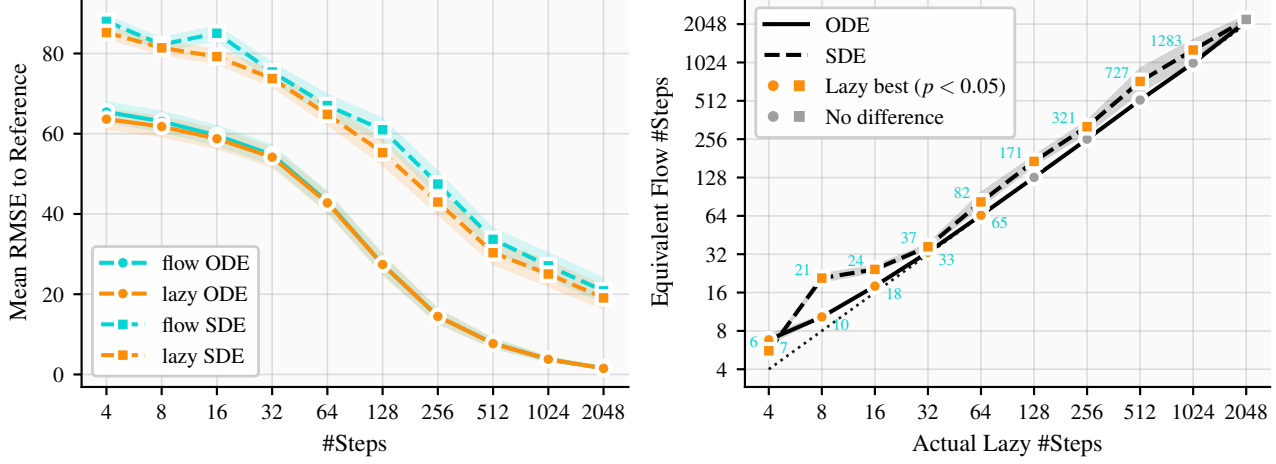


Figure 3. Left: Pixel-wise RMSE predictor-corrector convergence plot for ODE (circle markers and solid curves) and statistically optimal SDE (square markers and dashed curves) generation with the original linear `flow` model schedule versus the converted `lazy` schedule as in Figure 2. Average and 95% confidence interval (shaded bands) is over 100 prompts, initial conditions and Wiener process realizations. One sees that convergence is (almost) monotone as a function of the number of solver steps for all four configurations. Compare with Figure 8. **Right:** Visual answer to the question “Using n_i numerical solver steps with the lazy schedule, how many solver steps would I on average need to use with the linear flow model schedule to achieve the same RMSE to the reference image?”. The answer for each n_i on the x -axis is plotted on the y -axis (cyan labels indicate nearest rounded integer). Shaded bands indicate 95% confidence intervals. The lazy schedule almost always performs statistically significantly better (and never worse) for both ODE and SDE generation, but the improvement is much bigger for SDE generation. All confidence intervals are calculated by bootstrapping with 10,000 samples.

(Proposition B.1) so it is numerically undefined. To deal with this we sample the first step under the lazy schedule; this is easily shown to be equivalent to setting $X_{\Delta t}^* = \sqrt{(1 - \Delta t)^2 + (\Delta t)^2} W_{\Delta t}$ where $W_{\Delta t}$ is the initial increment of the fixed Wiener process.

In Figure 3 (left) we see that each of the four configurations converges more or less monotonically to its reference image, but convergence is significantly faster with ODE generation than with SDE generation, indicating the difficulty in numerically solving SDEs. See also Figure 8 showing that the two SDEs converge more slowly to a common reference image.

To test whether the effect of converting to the lazy schedule is statistically significantly positive for ODE and SDE generation, respectively, we ask the following question: “Using n_i numerical solver steps with the lazy schedule, how many solver steps would I on average need to use with the linear flow model schedule to achieve the same RMSE to the reference image?”. The answer to this question is illustrated in Figure 3 (right). For ODE integration the improvement is statistically significant up until $n_i = 64$ yet quite small; one saves at most three solver steps (which for $n_i = 4$ almost halves the sampling time) using the lazy schedule instead of the original linear flow model schedule. For SDE generation the improvement is much larger; for example, using 128 predictor-corrector steps with the lazy schedule achieves a performance (on average) similar to using 171 solver steps with the linear flow model schedule.

9. Discussion

We stress that since the PRX model outputs a learned approximation $\hat{v}^{\text{flow}} \approx v^{\text{flow}}$ the flow-to-lazy conversion is inexact as noted in Remark 7.7. The fact that the lazy schedule performs statistically better than the linear flow schedule that the PRX model was trained with is therefore very convincing and leads us to hypothesize that training a model from scratch using e.g. the lazy ODE schedule from Example 7.4 would lead to significantly bigger improvements in sampling quality.

We also stress that the slow convergence of the SDE does *not* allow us to conclude that the statistically optimal SDE generates poorer images than the ODE. The more interesting metric, which is harder to measure, is *distributional fit to the test dataset* and the tradeoff between that and ease of numerical integration for the ODE versus the SDE. We leave this to future work but note that the sample images in Appendix F indicate that using a moderate amount of solver steps (say $n_i \geq 64$) for the statistically optimal SDE generates aesthetically pleasing and detailed images, especially with the lazy schedule.

On the theoretical side it would be valuable to extend the lazy schedule family beyond the Gaussian data assumption. We hypothesize that for the statistically optimal SDE one will end up with a point mass schedule under reasonable assumptions on the data density ρ_X .

Software and Data

Code will be released upon acceptance.

Impact Statement

This paper presents work whose goal is to advance the field of Machine Learning. There are many potential societal consequences of our work, none which we feel must be specifically highlighted here.

References

Albergo, M., Boffi, N., Lindsey, M., and Vanden-Eijnden, E. Multimarginal generative modeling with stochastic interpolants. In Kim, B., Yue, Y., Chaudhuri, S., Fragkiadaki, K., Khan, M., and Sun, Y. (eds.), *International Conference on Learning Representations*, volume 2024, pp. 55884–55901, 2024.

Albergo, M., Boffi, N. M., and Vanden-Eijnden, E. Stochastic interpolants: A unifying framework for flows and diffusions. *Journal of Machine Learning Research*, 26 (209):1–80, 2025.

Almazán, J., Bertoin, D., and Frigg, R. We’re open-sourcing our text-to-image model and the process behind it. <https://huggingface.co/blog/Photoroom/prx-open-source-t2i-model>, November 2025.

Anderson, B. D. Reverse-time diffusion equation models. *Stochastic Processes and their Applications*, 12(3):313–326, 1982. doi: 10.1016/0304-4149(82)90051-5.

Boffi, N. M., Albergo, M. S., and Vanden-Eijnden, E. Flow map matching with stochastic interpolants: A mathematical framework for consistency models. *Transactions on Machine Learning Research*, 2025. ISSN 2835-8856.

Bortoli, V. D., Thornton, J., Heng, J., and Doucet, A. Diffusion schrödinger bridge with applications to score-based generative modeling. In Beygelzimer, A., Dauphin, Y., Liang, P., and Vaughan, J. W. (eds.), *Advances in Neural Information Processing Systems*, 2021.

Chen, X., Fang, H., Lin, T.-Y., Vedantam, R., Gupta, S., Dollar, P., and Zitnick, C. L. Microsoft coco captions: Data collection and evaluation server, 2015.

Chen, Y., Goldstein, M., Hua, M., Albergo, M. S., Boffi, N. M., and Vanden-Eijnden, E. Probabilistic forecasting with stochastic interpolants and föllmer processes. In Salakhutdinov, R., Kolter, Z., Heller, K., Weller, A., Oliver, N., Scarlett, J., and Berkenkamp, F. (eds.), *Proceedings of the 41st International Conference on Machine Learning*, volume 235 of *Proceedings of Machine Learning Research*, pp. 6728–6756. PMLR, 21–27 Jul 2024.

Chen, Y., Vanden-Eijnden, E., and Xu, J. Lipschitz-guided design of interpolation schedules in generative models, 2025.

Heusel, M., Ramsauer, H., Unterthiner, T., Nessler, B., and Hochreiter, S. Gans trained by a two time-scale update rule converge to a local nash equilibrium. In Guyon, I., Luxburg, U. V., Bengio, S., Wallach, H., Fergus, R., Vishwanathan, S., and Garnett, R. (eds.), *Advances in Neural Information Processing Systems*, volume 30. Curran Associates, Inc., 2017.

Ho, J. and Salimans, T. Classifier-free diffusion guidance. <https://arxiv.org/abs/2207.12598>, 2022.

Ho, J., Jain, A., and Abbeel, P. Denoising diffusion probabilistic models. In Larochelle, H., Ranzato, M., Hadsell, R., Balcan, M., and Lin, H. (eds.), *Advances in Neural Information Processing Systems*, volume 33, pp. 6840–6851. Curran Associates, Inc., 2020.

Karras, T., Aittala, M., Aila, T., and Laine, S. Elucidating the design space of diffusion-based generative models. In Koyejo, S., Mohamed, S., Agarwal, A., Belgrave, D., Cho, K., and Oh, A. (eds.), *Advances in Neural Information Processing Systems*, volume 35, pp. 26565–26577. Curran Associates, Inc., 2022.

Lai, C.-H., Song, Y., Kim, D., Mitsufuji, Y., and Ermon, S. The principles of diffusion models. *arXiv preprint arXiv:2510.21890*, 2025.

Le Gall, J.-F. *Brownian Motion, Martingales, and Stochastic Calculus*. Graduate Texts in Mathematics. Springer Cham, 1 edition, 2016. ISBN 978-3-319-31089-3. doi: 10.1007/978-3-319-31089-3.

Lin, T.-Y., Maire, M., Belongie, S., Hays, J., Perona, P., Ramanan, D., Dollár, P., and Zitnick, C. L. Microsoft coco: Common objects in context. In Fleet, D., Pajdla, T., Schiele, B., and Tuytelaars, T. (eds.), *Computer Vision – ECCV 2014*, pp. 740–755, Cham, 2014. Springer International Publishing.

Lipman, Y., Chen, R. T. Q., Ben-Hamu, H., Nickel, M., and Le, M. Flow matching for generative modeling. In *The Eleventh International Conference on Learning Representations*, 2023.

Liu, Q. Let us flow together. https://www.cs.utexas.edu/~lqiang/PDF/flow_book.pdf, December 2024. Working draft (dated December 24, 2024).

Liu, X., Gong, C., and Liu, Q. Flow straight and fast: Learning to generate and transfer data with rectified flow. In *The Eleventh International Conference on Learning Representations*, 2023.

Ma, N., Goldstein, M., Albergo, M. S., Boffi, N. M., Vandeneijnden, E., and Xie, S. Sit: Exploring flow and diffusion-based generative models with scalable interpolant transformers. In Leonardis, A., Ricci, E., Roth, S., Russakovsky, O., Sattler, T., and Varol, G. (eds.), *Computer Vision – ECCV 2024*, pp. 23–40, Cham, 2024. Springer Nature Switzerland. ISBN 978-3-031-72980-5.

Negrel, H., Coeurdoux, F., Albergo, M. S., and Vandeneijnden, E. Multitask learning with stochastic interpolants. In *Advances in Neural Information Processing Systems (NeurIPS 2025)*, 2025. Accepted to NeurIPS 2025 as a Spotlight; camera-ready hosted on OpenReview.

Nichol, A. Q. and Dhariwal, P. Improved denoising diffusion probabilistic models, 2021.

Photoroom. PRX: Open Text-to-Image Generative Model (prx-1024-t2i-beta). <https://huggingface.co/Photoroom/prx-1024-t2i-beta>, 2025. Hugging Face model card. Github commit ID: 84772b42065c4fffcfc10a7269e1aebf104fc0ef1.

Pooladian, A.-A. and Niles-Weed, J. Plug-in estimation of schrödinger bridges. *SIAM Journal on Mathematics of Data Science*, 7(3):1315–1336, 2025. doi: 10.1137/24M1687340.

Pooladian, A.-A., Ben-Hamu, H., Domingo-Enrich, C., Amos, B., Lipman, Y., and Chen, R. T. Q. Multisample flow matching: Straightening flows with minibatch couplings. In Krause, A., Brunskill, E., Cho, K., Engelhardt, B., Sabato, S., and Scarlett, J. (eds.), *Proceedings of the 40th International Conference on Machine Learning*, volume 202 of *Proceedings of Machine Learning Research*, pp. 28100–28127. PMLR, 23–29 Jul 2023.

Sabour, A., Fidler, S., and Kreis, K. Align your steps: optimizing sampling schedules in diffusion models. In *Proceedings of the 41st International Conference on Machine Learning*, ICML’24. JMLR.org, 2024.

Salimans, T., Goodfellow, I., Zaremba, W., Cheung, V., Radford, A., Chen, X., and Chen, X. Improved techniques for training gans. In Lee, D., Sugiyama, M., Luxburg, U., Guyon, I., and Garnett, R. (eds.), *Advances in Neural Information Processing Systems*, volume 29. Curran Associates, Inc., 2016.

Shi, Y., De Bortoli, V., Campbell, A., and Doucet, A. Diffusion schrödinger bridge matching. In Oh, A., Naumann, T., Globerson, A., Saenko, K., Hardt, M., and Levine, S. (eds.), *Advances in Neural Information Processing Systems*, volume 36, pp. 62183–62223. Curran Associates, Inc., 2023.

Sohl-Dickstein, J., Weiss, E., Maheswaranathan, N., and Ganguli, S. Deep unsupervised learning using nonequilibrium thermodynamics. In Bach, F. and Blei, D. (eds.), *Proceedings of the 32nd International Conference on Machine Learning*, volume 37 of *Proceedings of Machine Learning Research*, pp. 2256–2265, Lille, France, 07–09 Jul 2015. PMLR.

Song, Y. and Ermon, S. Generative modeling by estimating gradients of the data distribution. In Wallach, H., Larochelle, H., Beygelzimer, A., d’Alché-Buc, F., Fox, E., and Garnett, R. (eds.), *Advances in Neural Information Processing Systems*, volume 32. Curran Associates, Inc., 2019.

Song, Y. and Ermon, S. Improved techniques for training score-based generative models. In Larochelle, H., Ranzato, M., Hadsell, R., Balcan, M., and Lin, H. (eds.), *Advances in Neural Information Processing Systems*, volume 33, pp. 12438–12448. Curran Associates, Inc., 2020.

Song, Y., Sohl-Dickstein, J., Kingma, D. P., Kumar, A., Ermon, S., and Poole, B. Score-based generative modeling through stochastic differential equations. In *International Conference on Learning Representations*, 2021.

Song, Y., Dhariwal, P., Chen, M., and Sutskever, I. Consistency models. In Krause, A., Brunskill, E., Cho, K., Engelhardt, B., Sabato, S., and Scarlett, J. (eds.), *Proceedings of the 40th International Conference on Machine Learning*, volume 202 of *Proceedings of Machine Learning Research*, pp. 32211–32252. PMLR, 23–29 Jul 2023.

Stein, C. M. Estimation of the Mean of a Multivariate Normal Distribution. *The Annals of Statistics*, 9(6):1135 – 1151, 1981. doi: 10.1214/aos/1176345632.

Xue, S., Liu, Z., Chen, F., Zhang, S., Hu, T., Xie, E., and Li, Z. Accelerating diffusion sampling with optimized time steps. In *2024 IEEE/CVF Conference on Computer Vision and Pattern Recognition (CVPR)*, pp. 8292–8301, 2024. doi: 10.1109/CVPR52733.2024.00792.

A. Proofs

Proposition 4.2 (intra-interpolant conversion formulas). *For a fixed interpolation schedule (α, β) and non-negative $\varepsilon \in C^1([0, 1])$, each of the functions $\eta_Z, \eta_X, s, b^\varepsilon$ uniquely defines all of the others on $(0, 1) \times \mathbb{R}^d$. In particular, each function can be expressed in terms of the score as*

$$\begin{aligned}\eta_Z(t, x) &= -\alpha_t s(t, x), \\ \eta_X(t, x) &= (x + \alpha_t^2 s(t, x)) / \beta_t, \\ b^\varepsilon(t, x) &= (\varepsilon_t^* + \varepsilon_t) s(t, x) + (\dot{\beta}_t / \beta_t) x.\end{aligned}$$

Proof. For $t \in (0, 1)$ we can clearly isolate the score s in each of the relations in the proposition. It therefore suffices to prove that each of the relations hold for all $(t, x) \in (0, 1) \times \mathbb{R}^d$, as claimed.

The first relation is a standard result that can be proved with Stein's lemma (also known as *Gaussian integration by parts*) (Stein, 1981) saying that $s(t, x) = -\eta_Z(t, x) / \alpha_t$ for $(t, x) \in [0, 1] \times \mathbb{R}^d$, see e.g. Theorem 8 in Albergo et al. (2025). The second relation follows easily from the definition of the stochastic interpolant (Definition 1.1) $I_t = \alpha_t Z + \beta_t X$ and linearity of expectation. Indeed, taking expectations conditional on $I_t = x$ in the definition for I_t gives

$$\eta_X(t, x) = \frac{1}{\beta_t} (x - \alpha_t \eta_Z(t, x)) = \frac{1}{\beta_t} (x + \alpha_t^2 s(t, x)),$$

where we used the first relation to get the last equality.

To get the final relation, plug the preceding relations into the definition of the drift

$$\begin{aligned}b^\varepsilon(t, x) &= \dot{\alpha}_t \eta_Z(t, x) + \dot{\beta}_t \eta_X(t, x) + \varepsilon_t s(t, x) \\ &= \dot{\alpha}_t (-\alpha_t s(t, x)) + \dot{\beta}_t \left(\frac{1}{\beta_t} (x + \alpha_t^2 s(t, x)) \right) + \varepsilon_t s(t, x) \\ &= \left(\alpha_t^2 \frac{\dot{\beta}_t}{\beta_t} - \alpha_t \dot{\alpha}_t + \varepsilon_t \right) s(t, x) + \frac{\dot{\beta}_t}{\beta_t} x.\end{aligned}$$

Since by Definition 4.1 $\varepsilon_t^* = \alpha_t^2 \dot{\beta}_t / \beta_t - \alpha_t \dot{\alpha}_t$ this concludes the proof of the proposition. \square

Theorem 4.3. *Assume we are given statistically learnt estimates $\hat{\eta}_Z, \hat{\eta}_X, \hat{s}$ or \hat{b}^ε of the true functions from Definition 1.3 with remaining estimates given by Proposition 4.2. Let X_t^ε solve the SDE (1) and consider the plug-in SDE*

$$d\hat{X}_t^\varepsilon = \hat{b}^\varepsilon(t, \hat{X}_t^\varepsilon) dt + \sqrt{2\varepsilon_t} dW_t,$$

solved forward in time t with $\hat{X}_0^\varepsilon \sim \mathcal{N}(0, \mathbf{I})$ independent of W . Then the minimizer of the Kullback-Leibler divergence between the path measures of X^ε and \hat{X}^ε over the diffusion scale ε is

$$\operatorname{argmin}_{\varepsilon \geq 0, \varepsilon \in C^1((0, 1])} \text{KL}\left(X^\varepsilon, \hat{X}^\varepsilon\right) = \varepsilon^*,$$

and the minimum is

$$\text{KL}\left(X^{\varepsilon^*}, \hat{X}^{\varepsilon^*}\right) = \int_0^1 \varepsilon_t^* \mathbb{E}[\|s(t, I_t) - \hat{s}(t, I_t)\|^2] dt.$$

Proof. An application of Girsanov's theorem gives

$$\begin{aligned}\text{KL}(X^\varepsilon, \hat{X}^\varepsilon) &= \frac{1}{4} \int_0^1 \frac{1}{\varepsilon_t} \mathbb{E}[\|b^\varepsilon(t, X_t^\varepsilon) - \hat{b}^\varepsilon(t, X_t^\varepsilon)\|^2] dt \\ &= \frac{1}{4} \int_0^1 \frac{1}{\varepsilon_t} \mathbb{E}[\|b^\varepsilon(t, I_t) - \hat{b}^\varepsilon(t, I_t)\|^2] dt \\ &= \frac{1}{4} \int_0^1 \frac{(\varepsilon_t^* + \varepsilon_t)^2}{\varepsilon_t} \mathbb{E}[\|s(t, I_t) - \hat{s}(t, I_t)\|^2] dt,\end{aligned}$$

where in the second equality we used that $\text{Law } X_t^\varepsilon = \text{Law } I_t$ and in the third equality we used Proposition 4.2 with the assumptions on \hat{b} and \hat{s} in this theorem. From the last expression we see that minimizing the KL-divergence over the diffusion scale ε amounts to minimizing the expression $(\varepsilon_t^* + \varepsilon_t)^2/\varepsilon_t$ over ε_t for all $t \in [0, 1]$ since the expectation term does not depend on ε_t . Differentiating this expression with respect to ε_t and setting the resulting expression to zero gives the (unique) minimizer $\varepsilon_t = \varepsilon_t^*$ for all $t \in [0, 1]$, and the theorem follows. \square

Proposition 5.2. *For the linear interpolant \bar{I}_t from Definition 5.1 it holds that $\bar{\varepsilon}_t^* = (1-t)/t$. Therefore*

$$\int_s^t 2\bar{\varepsilon}_u^* du = 2(\log(t) - t - \log(s) + s)$$

for $0 < s \leq t \leq 1$ and the integral is infinite for $s = 0$.

Proof. We have $\bar{\alpha}_t = 1-t$, $\bar{\beta}_t = t$ so that $\dot{\bar{\alpha}}_t = -1$ and $\dot{\bar{\beta}}_t = 1$. Thus

$$\bar{\varepsilon}_t^* = \bar{\alpha}_t^2 \frac{\dot{\bar{\beta}}_t}{\bar{\beta}_t} - \bar{\alpha}_t \dot{\bar{\alpha}}_t = \frac{(1-t)^2}{t} + (1-t) = \frac{1-t}{t}.$$

The rest of the proposition easily follows. \square

Recall Definition 5.3.

Definition 5.3. For $t \in [0, 1]$ we define the functions

$$c_t := \alpha_t + \beta_t, \quad u_t := \beta_t/c_t.$$

For the remaining proofs we will often reference the following lemma with some useful algebraic identities.

Lemma A.1. *For $t \in (0, 1]$ the following identities hold.*

$$1 - u_t = \frac{\alpha_t}{c_t}, \tag{2}$$

$$\frac{\dot{u}_t}{u_t} = \frac{\dot{\beta}_t}{\beta_t} - \frac{\dot{c}_t}{c_t} = \frac{\varepsilon_t^*}{\alpha_t c_t}. \tag{3}$$

Proof. Equation (2) is trivial:

$$1 - u_t = \frac{c_t - \beta_t}{c_t} = \frac{\alpha_t}{c_t}.$$

To get the leftmost equality in Equation (3), observe that

$$\dot{u}_t = \frac{\dot{\beta}_t c_t - \beta_t \dot{c}_t}{c_t^2},$$

so

$$\frac{\dot{u}_t}{u_t} = \frac{\dot{\beta}_t c_t - \beta_t \dot{c}_t}{c_t \beta_t} = \frac{\dot{\beta}_t}{\beta_t} - \frac{\dot{c}_t}{c_t}.$$

Finally,

$$c_t \frac{\dot{u}_t}{u_t} = \alpha_t \frac{\dot{\beta}_t}{\beta_t} + \dot{\beta}_t - \dot{\alpha}_t - \dot{\beta}_t = \frac{\varepsilon_t^*}{\alpha_t},$$

which proves the rightmost equality in Equation (3). \square

Proposition 5.4 (inter-conversion formulas). *For a schedule (α, β) and non-negative $\varepsilon \in C^1([0, 1])$, the functions $\eta_Z, \eta_X, s, b^\varepsilon$ are uniquely defined from any of the functions $\bar{\eta}_Z, \bar{\eta}_X, \bar{s}, \bar{b}^\varepsilon$ associated with the linear interpolant. In particular,*

$$\eta_Z(t, x) = \bar{\eta}_Z(u_t, x/c_t), \quad \eta_X(t, x) = \bar{\eta}_X(u_t, x/c_t),$$

$$s(t, x) = (1/c_t) \bar{s}(u_t, x/c_t),$$

$$b^\varepsilon(t, x) = \frac{\dot{c}_t}{c_t} x + c_t \dot{u}_t \bar{b}^\varepsilon \left(u_t, \frac{x}{c_t} \right) \quad \text{for } \bar{\varepsilon}_{u_t} = \frac{\alpha_t \varepsilon_t}{\beta_t \varepsilon_t^*}.$$

Proof. Using Equation (2) we get

$$\begin{aligned}\bar{\eta}_Z\left(u_t, \frac{x}{c_t}\right) &= \mathbb{E}\left[Z \mid (1-u_t)Z + u_tX = \frac{x}{c_t}\right] \\ &= \mathbb{E}\left[Z \mid \frac{\alpha_t}{c_t}Z + \frac{\beta_t}{c_t}X = \frac{x}{c_t}\right] \\ &= \mathbb{E}[Z \mid \alpha_tZ + \beta_tX = x] \\ &= \eta_Z(t, x).\end{aligned}$$

An analogous derivation proves $\eta_X(t, x) = \bar{\eta}_X(u_t, x/c_t)$.

From the relation $s(t, x) = -(1/\alpha_t)\eta_Z(t, x)$ (as in Proposition 4.2) combined with $\eta_Z(t, x) = \bar{\eta}_Z(u_t, x/c_t)$ we get

$$\bar{s}\left(u_t, \frac{x}{c_t}\right) = -\frac{1}{1-u_t}\bar{\eta}_Z\left(u_t, \frac{x}{c_t}\right) = -\frac{1}{1-u_t}\eta_Z(t, x).$$

Observing that $1/(1-u_t) = c_t/\alpha_t$ we get

$$\frac{1}{c_t}\bar{s}\left(u_t, \frac{x}{c_t}\right) = -\frac{1}{\alpha_t}\eta_Z(t, x) = s(t, x),$$

as claimed.

Getting the final relation requires a bit more work, but the overall strategy is the same as for the above; we first convert the drift to the score, then the score to the linear score, and then the linear score to the linear drift using the particular linear diffusion scale $\bar{\varepsilon}_{u_t} = (\alpha_t\varepsilon_t)/(\beta_t\varepsilon_t^*)$. To be precise, we first apply Proposition 4.2, then the relation we just proved, and then Proposition 4.2 again to get

$$\begin{aligned}b^\varepsilon(t, x) &= (\varepsilon_t^* + \varepsilon_t)s(t, x) + \frac{\dot{\beta}_t}{\beta_t}x \\ &= \frac{\varepsilon_t^* + \varepsilon_t}{c_t}\bar{s}(u_t, \frac{x}{c_t}) + \frac{\dot{\beta}_t}{\beta_t}x \\ &= \frac{\varepsilon_t^* + \varepsilon_t}{c_t}\left(\frac{\bar{b}^{\bar{\varepsilon}}\left(u_t, \frac{x}{c_t}\right) - \frac{x}{u_t c_t}}{\bar{\varepsilon}_{u_t}^* + \bar{\varepsilon}_{u_t}}\right) + \frac{\dot{\beta}_t}{\beta_t}x.\end{aligned}$$

We now plug in the linear diffusion scale $\bar{\varepsilon}_{u_t} = (\alpha_t\varepsilon_t)/(\beta_t\varepsilon_t^*)$, which we motivate in the proof of Theorem 5.5. By Proposition 5.2 and Equation (2) we get $\bar{\varepsilon}_{u_t}^* = (1-u_t)/u_t = \alpha_t/\beta_t$ so that

$$\bar{\varepsilon}_{u_t}^* + \bar{\varepsilon}_{u_t} = \frac{\alpha_t}{\beta_t}\left(\frac{\varepsilon_t^* + \varepsilon_t}{\varepsilon_t^*}\right).$$

Thus

$$\begin{aligned}b^\varepsilon(t, x) &= \frac{\beta_t\varepsilon_t^*}{\alpha_t c_t}\left(\bar{b}^{\bar{\varepsilon}}\left(u_t, \frac{x}{c_t}\right) - \frac{x}{u_t c_t}\right) + \frac{\dot{\beta}_t}{\beta_t}x \\ &= c_t \dot{u}_t \left(\bar{b}^{\bar{\varepsilon}}\left(u_t, \frac{x}{c_t}\right) - \frac{x}{u_t c_t}\right) + \frac{\dot{\beta}_t}{\beta_t}x \quad (\text{using Equation (3)}) \\ &= c_t \dot{u}_t \bar{b}^{\bar{\varepsilon}}\left(u_t, \frac{x}{c_t}\right) + \left(\frac{\dot{\beta}_t}{\beta_t} - \frac{\dot{u}_t}{u_t}\right)x \\ &= c_t \dot{u}_t \bar{b}^{\bar{\varepsilon}}\left(u_t, \frac{x}{c_t}\right) + \frac{\dot{c}_t}{c_t}x. \quad (\text{using Equation (3)})\end{aligned}$$

This concludes the proof. \square

Theorem 5.5 (pathwise conversion). *Let (α, β) be a schedule satisfying the requirements in Definition 1.1, let $z \in \mathbb{R}^d$ and let $(W_t)_{t \in [0,1]}$ be a Wiener process realization. Let X_t^ε solve the SDE (1) in physical time t from $X_0^\varepsilon = z$ driven by W with diffusion scale ε . Let $\bar{X}_u^{\bar{\varepsilon}}$ solve the SDE (1) with linear schedule in reparameterized time $u = u_t$ from $\bar{X}_0^{\bar{\varepsilon}} = z$ driven by*

$$\bar{W}_u = \int_0^{t_u} \sqrt{\dot{u}_s} dW_s, \quad u \in [0, 1]$$

with diffusion scale $\bar{\varepsilon}_u = (\alpha_{t_u} \varepsilon_{t_u}) / (\beta_{t_u} \varepsilon_{t_u}^)$. Then the solution X_t^ε can be obtained from the solution $\bar{X}_{u_t}^{\bar{\varepsilon}}$ associated with the linear interpolant via the formula*

$$X_t^\varepsilon = c_t \bar{X}_{u_t}^{\bar{\varepsilon}}, \quad t \in [0, 1].$$

In particular, $X_1^\varepsilon = \bar{X}_1^{\bar{\varepsilon}}$ (since $c_1 = 1$).

Proof. First of all we note that \bar{W} is indeed a Wiener process in reparameterized time $u = u_t$ by Lévy's characterization theorem (see e.g. Theorem 5.12 in Le Gall (2016)) since it has quadratic variation $\langle \bar{W} \rangle_u = \int_0^{t_u} \dot{u}_s ds = \int_0^u du = u$. Thus both SDEs in the theorem statement are well-defined with unique solutions, so it suffices to prove that their dynamics coincide i.e. that $dX_t^\varepsilon = d(c_t \bar{X}_{u_t}^{\bar{\varepsilon}})$ for all $t \in (0, 1)$. By the Itô product rule, the latter infinitesimal is

$$\begin{aligned} d(c_t \bar{X}_{u_t}^{\bar{\varepsilon}}) &= \dot{c}_t \bar{X}_{u_t}^{\bar{\varepsilon}} dt + c_t \bar{b}^{\bar{\varepsilon}}(u_t, \bar{X}_{u_t}^{\bar{\varepsilon}}) du_t + c_t \sqrt{2\bar{\varepsilon}_{u_t}} d\bar{W}_{u_t} \\ &= \dot{c}_t \bar{X}_{u_t}^{\bar{\varepsilon}} dt + c_t \dot{u}_t \bar{b}^{\bar{\varepsilon}}(u_t, \bar{X}_{u_t}^{\bar{\varepsilon}}) dt + c_t \sqrt{2\bar{\varepsilon}_{u_t} \dot{u}_t} dW_t. \end{aligned}$$

Using the linear diffusion scale $\bar{\varepsilon}_{u_t} = (\alpha_{t_u} \varepsilon_t) / (\beta_{t_u} \varepsilon_t^*)$ with Equation (3) gives

$$\bar{\varepsilon}_{u_t} = \frac{u_t}{\dot{u}_t} \frac{\varepsilon_t}{\beta_t c_t} = \frac{\varepsilon_t}{c_t^2 \dot{u}_t},$$

which we plug into the above infinitesimal to arrive at

$$d(c_t \bar{X}_{u_t}^{\bar{\varepsilon}}) = \dot{c}_t \bar{X}_{u_t}^{\bar{\varepsilon}} dt + c_t \dot{u}_t \bar{b}^{\bar{\varepsilon}}(u_t, \bar{X}_{u_t}^{\bar{\varepsilon}}) dt + \sqrt{2\bar{\varepsilon}_t} dW_t.$$

Using now Proposition 5.4 we see that

$$dX_t^\varepsilon = b^\varepsilon(t, X_t^\varepsilon) dt + \sqrt{2\varepsilon_t} dW_t = \frac{\dot{c}_t}{c_t} X_t^\varepsilon dt + c_t \dot{u}_t \bar{b}^{\bar{\varepsilon}}\left(u_t, \frac{X_t^\varepsilon}{c_t}\right) dt + \sqrt{2\varepsilon_t} dW_t,$$

which after inserting the theorem's ansatz $X_t^\varepsilon / c_t = \bar{X}_{u_t}^{\bar{\varepsilon}}$ shows that $dX_t^\varepsilon = d(c_t \bar{X}_{u_t}^{\bar{\varepsilon}})$. This concludes the proof. \square

To prove Theorem 6.3 we first state and prove a useful lemma.

Lemma A.2. *For any point mass schedule (α, β) it holds that*

$$u_0 := \lim_{t \rightarrow 0_+} u_t = 0 \iff \beta_t = o(\alpha_t) \quad \text{as} \quad t \rightarrow 0_+.$$

Proof. We have that

$$u_0 := \lim_{t \rightarrow 0_+} u_t = \lim_{t \rightarrow 0_+} \frac{\beta_t}{\alpha_t + \beta_t} = \lim_{t \rightarrow 0_+} \frac{1}{1 + \frac{\alpha_t}{\beta_t}}.$$

Clearly this limit is zero if and only if the ratio $\alpha_t / \beta_t \rightarrow \infty$ as $t \rightarrow 0_+$, or equivalently if and only if $\beta_t = o(\alpha_t)$ as $t \rightarrow 0_+$. \square

Theorem 6.3. *Let (α, β) be a point mass schedule as in Definition 6.1. Then given any non-negative bounded diffusion scale $\varepsilon \in C^1([0, 1])$, the SDE (1) is well-defined in the classical sense for $t \in (0, 1]$ with initial position $X_0^\varepsilon = 0$, and the initial drift is well-defined in distribution. It holds that $\text{Law}(X_t^\varepsilon) = \text{Law}(I_t)$ for all $t \in [0, 1]$ and Theorem 5.5 still applies: in particular, the point mass SDE solution and initial drift relates to the solution and initial condition of the linear interpolant as $X_t^\varepsilon = c_t \bar{X}_{u_t}^{\bar{\varepsilon}}$ for $t \in [0, 1]$ and $b^\varepsilon(0, X_0^\varepsilon) = (\dot{c}_0 - \lim_{t \rightarrow 0_+} (\varepsilon_t / \alpha_t)) \bar{X}_0^{\bar{\varepsilon}}$.*

Proof. Since the point mass schedule from Definition 6.1 only differs from the regular schedule from Definition 1.1 at $t = 0$ this is the only case we need to consider. In particular, Theorem 5.5 holds on $(0, 1]$ and also in the limit as $t \rightarrow 0_+$ since from the boundary conditions $\alpha_0 = \beta_0 = 0$ we have $c_0 = u_0 = 0$ so that $X_0^\varepsilon = c_0 \bar{X}_0^\varepsilon = 0$ for all $(z, \omega) \in \mathbb{R}^d \times \Omega$ with $z = \bar{X}_0^\varepsilon$ the initial condition to the linear interpolant and ω an event in the probability space of the shared Wiener process.

Substituting now $c_t x$ for x in Proposition 5.4 gives the conversion formula

$$b^\varepsilon(t, c_t x) = \dot{c}_t x + c_t \dot{u}_t \bar{b}^\varepsilon(u_t, x),$$

for all $(t, x) \in (0, 1) \times \mathbb{R}^d$ with $\bar{\varepsilon}_{u_t} = \frac{\alpha_t \varepsilon_t}{\beta_t \varepsilon_t^*}$. Going to the limit gives us

$$\lim_{t \rightarrow 0_+} b^\varepsilon(t, c_t x) = \lim_{t \rightarrow 0_+} \dot{c}_t x + \lim_{t \rightarrow 0_+} c_t \dot{u}_t \bar{b}^\varepsilon(u_t, x),$$

so it remains to prove that $\lim_{t \rightarrow 0_+} c_t \dot{u}_t \bar{b}^\varepsilon(u_t, x) = -\lim_{t \rightarrow 0_+} (\varepsilon_t / \alpha_t) x$ under our assumptions in Definition 6.1. To this end we first consider the expression for the drift of the linear interpolant,

$$\begin{aligned} \bar{b}^\varepsilon(u_t, x) &= (\bar{\varepsilon}_{u_t}^* + \bar{\varepsilon}_{u_t}) \bar{s}(u_t, x) + \frac{\dot{\bar{\beta}}_{u_t}}{\bar{\beta}_{u_t}} x && \text{(by Proposition 4.2)} \\ &= \left(\frac{1 - u_t}{u_t} + \frac{\alpha_t \varepsilon_t}{\beta_t \varepsilon_t^*} \right) \left(-\frac{\bar{\eta}_Z(u_t, x)}{1 - u_t} \right) + \frac{1}{u_t} x && \text{(by Proposition 4.2 and Proposition 5.2)} \\ &= -\frac{\alpha_t}{\beta_t} \left(1 + \frac{\varepsilon_t}{\varepsilon_t^*} \right) \frac{\bar{\eta}_Z(u_t, x) c_t}{\alpha_t} + \frac{c_t}{\beta_t} x && \text{(by Equation (2))} \\ &= \frac{c_t}{\beta_t} \left(x - \bar{\eta}_Z(u_t, x) - \frac{\varepsilon_t}{\varepsilon_t^*} \bar{\eta}_Z(u_t, x) \right) \\ &= \frac{c_t}{\beta_t} (x - \bar{\eta}_Z(u_t, x)) - \frac{u_t \varepsilon_t}{\dot{u}_t \alpha_t \beta_t} \bar{\eta}_Z(u_t, x) && \text{(by Equation (3))} \\ &= \frac{c_t}{\beta_t} (x - \bar{\eta}_Z(u_t, x)) - \frac{\varepsilon_t}{\dot{u}_t \alpha_t c_t} \bar{\eta}_Z(u_t, x). \end{aligned}$$

Multiplying by $c_t \dot{u}_t$ and going to the limit with the assumptions on the point mass schedule (α, β) from Definition 6.1 finally gives

$$\begin{aligned} c_t \dot{u}_t \bar{b}^\varepsilon(u_t, x) &= \frac{c_t^2 \dot{u}_t}{\beta_t} (x - \bar{\eta}_Z(u_t, x)) - \frac{\varepsilon_t}{\alpha_t} \bar{\eta}_Z(u_t, x) \\ &\rightarrow -\lim_{t \rightarrow 0_+} \frac{\varepsilon_t}{\alpha_t} x \quad \text{as } t \rightarrow 0_+, \end{aligned}$$

where to get the limit we used that $\bar{\eta}_Z(u_t, x) = \mathbb{E}[Z \mid \bar{I}_{u_t} = x] \rightarrow x$ as $t \rightarrow 0_+$ since $u_0 = 0, \dot{u}_0 < \infty$ (and $\bar{I}_0 = Z$), as well as $c_t^2 \dot{u}_t / \beta_t = \dot{u}_t (\alpha_t^2 + \beta_t^2 + 2\alpha_t \beta_t) / \beta_t \rightarrow \alpha_t^2 \dot{u}_t / \beta_t \rightarrow C$ as $t \rightarrow 0_+$ for some non-negative bounded constant $C \in \mathbb{R}_+$ since $\dot{u}_0 < \infty, \alpha_0 = \beta_0 = 0$, and since the point mass schedule is assumed to satisfy $\alpha_t^2 = O(\beta_t)$ as $t \rightarrow 0_+$. This concludes the proof.

We note that the point mass schedule assumption $\alpha_t^2 = O(\beta_t)$ as $t \rightarrow 0_+$ can be relaxed, but this comes at the expense of requiring $\bar{\eta}_Z(u_t, x)$ to converge sufficiently fast to x as $t \rightarrow 0_+$ so that the limiting product $\lim_{t \rightarrow 0_+} ((\alpha_t^2 \dot{u}_t) / \beta_t)(x - \bar{\eta}_Z(u_t, x))$ still goes to zero. To the best of our knowledge, this requires assuming that the data distribution ρ_X has sufficiently light tails; see Assumption B.3 and Theorem B.4 in Chen et al. (2024). We feel like our assumption is simpler, and for what is done in this paper the assumption $\alpha_t^2 = O(\beta_t)$ as $t \rightarrow 0_+$ is not prohibitively restrictive. \square

Proposition 6.5. *Let (α, β) be any valid schedule, possibly a point mass schedule. Then under the assumptions in Theorem 4.3, the minimal path-measure KL-divergence attained when $\varepsilon = \varepsilon^*$ is invariant to the choice of schedule.*

Proof. This is essentially already proved in Proposition 2.5 in Chen et al. (2025) whose proof we restate below using the notation of this paper. Recall that under the assumptions in Theorem 4.3, the minimum Kullback-Leibler divergence between the path measures of X^ε and \hat{X}^ε over the diffusion scale ε is

$$\text{KL}\left(X^{\varepsilon^*}, \hat{X}^{\varepsilon^*}\right) = \int_0^1 \varepsilon_t^* \mathbb{E}[\|s(t, I_t) - \hat{s}(t, I_t)\|^2] dt.$$

Define now the time change $\eta : [0, 1] \rightarrow \overline{\mathbb{R}}_+$ by $\eta_t := \alpha_t/\beta_t$, let ρ_η be the probability density function of the random variable $Y = X + \eta Z$ for $\eta \in [0, \infty]$ and denote by $s(\eta, y)$ the score of Y ⁷. Since from Definition 1.1 we can write $I_t = \alpha_t Z + \beta_t X = \beta_t(X + \eta_t Z) = \beta_t Y$ we see that the scores are related as

$$s(t, x) = \nabla \log \rho_t(x) = \frac{1}{\beta_t} \nabla \log \rho_\eta \left(\frac{x}{\beta_t} \right) = \frac{1}{\beta_t} s \left(\eta, \frac{x}{\beta_t} \right),$$

and similarly we have that the score estimates are related as $\hat{s}(t, x) = \hat{s}(\eta, x/\beta)/\beta_t$. Substituting the score of Y for the score of I in the expression for the KL-minimum gives

$$\begin{aligned} \text{KL} \left(X^{\varepsilon^*}, \hat{X}^{\varepsilon^*} \right) &= \int_0^1 \frac{\varepsilon_t^*}{\beta_t^2} \mathbb{E} \left[\left\| s \left(\eta_t, \frac{I_t}{\beta_t} \right) - \hat{s} \left(\eta_t, \frac{I_t}{\beta_t} \right) \right\|^2 \right] dt \\ &= \int_0^1 \frac{\varepsilon_t^*}{\beta_t^2} \mathbb{E} \left[\|s(\eta_t, Y) - \hat{s}(\eta_t, Y)\|^2 \right] dt. \end{aligned}$$

Noting that

$$\frac{\varepsilon_t^*}{\beta_t^2} = \frac{\alpha_t^2}{\beta_t^2} \left(\frac{\dot{\beta}_t}{\beta_t} - \frac{\dot{\alpha}_t}{\alpha_t} \right) = -\frac{\alpha_t}{\beta_t} \frac{d}{dt} \left(\frac{\alpha_t}{\beta_t} \right) = -\eta_t \dot{\eta}_t,$$

we change the integration variable from t to η in the KL-expression to get

$$\text{KL} \left(X^{\varepsilon^*}, \hat{X}^{\varepsilon^*} \right) = \int_{\eta_1}^{\eta_0} \eta \mathbb{E} \left[\|s(\eta, Y) - \hat{s}(\eta, Y)\|^2 \right] d\eta = \int_0^\infty \eta \mathbb{E} \left[\|s(\eta, Y) - \hat{s}(\eta, Y)\|^2 \right] d\eta.$$

Crucially, we substituted $\eta_1 = 0$ but also $\eta_0 := \lim_{t \rightarrow 0_+} \eta_t = \infty$ in the last expression, as in the original proof. We stress that $\eta_0 = \infty$ holds even for a point mass schedule since in Definition 6.1 we require $\beta_t = o(\alpha_t)$ as $t \rightarrow 0_+$, which is equivalent to requiring $u_0 = 0$ by Lemma A.2. This requirement cannot be relaxed without making the initial law of the resulting interpolant dependent on ρ_X , which is what we are trying to sample in the first place. Since the final expression for the KL-minimum is independent of the schedule (α, β) , the proof is concluded. \square

Proposition 7.1 (lazy schedule families). *Assume that $X \sim \mathcal{N}(0, \mathbf{I})$. Then for all $(t, x) \in [0, 1] \times \mathbb{R}^d$ it holds that*

1.

$$b(t, x) = 0 \iff \alpha_t^2 + \beta_t^2 = 1.$$

In words, the ODE velocity is identically zero if and only if the schedule is variance preserving.

2.

$$b^*(t, x) = 0 \iff \alpha_t^2 + \beta_t^2 = \beta_t.$$

This implies $\alpha_0 = 0, \beta_t = o(\alpha_t), \alpha_t^2 = O(\beta_t)$ as $t \rightarrow 0_+$. We have that $\dot{u}_0 < \infty \iff \dot{\beta}_t = O(\sqrt{\beta_t})$ in which case the schedule is a point mass schedule per Definition 6.1. It also holds for all $t \in [0, 1]$ that $\varepsilon_t^ = \dot{\beta}_t/2$ so that*

$$\int_s^t 2\varepsilon_u^* du = \beta_t - \beta_s \quad \text{for } 0 \leq s \leq t \leq 1.$$

Proof. Under the assumption $X \sim \mathcal{N}(0, \mathbf{I})$ it holds that $I_t \sim \mathcal{N}(0, (\alpha_t^2 + \beta_t^2) \mathbf{I})$ so that $s(t, x) = -x/(\alpha_t^2 + \beta_t^2)$. We first consider what this entails for the ODE case and then for the SDE case. It suffices to consider the condition $b(t, x) = 0$ for all $(t, x) \in (0, 1) \times \mathbb{R}^d$ since by continuity the condition $b(t, x) = 0$ for all $(t, x) \in [0, 1] \times \mathbb{R}^d$ is then covered too.

From Proposition 4.2 with $\varepsilon \equiv 0$ we see that requiring $b(t, x) = 0$ for all $(t, x) \in (0, 1) \times \mathbb{R}^d$ is equivalent to requiring $\varepsilon_t^* s(t, x) + \dot{\beta}_t/\beta_t x = 0$ for all $(t, x) \in (0, 1) \times \mathbb{R}^d$. This is equivalent to

$$\frac{\dot{\beta}_t}{\beta_t} - \frac{\varepsilon_t^*}{\alpha_t^2 + \beta_t^2} = 0 \quad \forall t \in (0, 1),$$

⁷We are abusing notation here, but in this proof it will always be clear from the argument (t or η) whether we are talking about the density of I or Y .

which by multiplying by $\alpha_t^2 + \beta_t^2$ is equivalent to

$$\varepsilon_t^* = \alpha_t^2 \frac{\dot{\beta}_t}{\beta_t} + \beta_t \dot{\beta}_t \quad \forall t \in (0, 1),$$

which from Definition 4.1 is again equivalent to

$$\alpha_t \dot{\alpha}_t = -\beta_t \dot{\beta}_t \quad \forall t \in (0, 1).$$

This is also equivalent to

$$\frac{d}{dt}(\alpha_t^2 + \beta_t^2) = C \quad \forall t \in (0, 1),$$

for some constant C . The boundary conditions $\alpha_1 = \beta_0 = 0, \alpha_0 = \beta_1 = 1$ then give $\alpha_t^2 + \beta_t^2 = 1$, proving the ODE case.

Next, we consider the SDE case. Here we use Proposition 4.2 with $\varepsilon = \varepsilon^*$ to see that requiring $b^*(t, x) = 0$ for all $(t, x) \in (0, 1) \times \mathbb{R}^d$ is equivalent to requiring $2\varepsilon_t^* s(t, x) + \dot{\beta}_t / \beta_t x = 0$ for all $(t, x) \in (0, 1) \times \mathbb{R}^d$. This is equivalent to

$$\frac{\dot{\beta}_t}{\beta_t} - \frac{2\varepsilon_t^*}{\alpha_t^2 + \beta_t^2} = 0 \quad \forall t \in (0, 1),$$

which by multiplying by $\alpha_t^2 + \beta_t^2$ is equivalent to

$$2\varepsilon_t^* = \alpha_t^2 \frac{\dot{\beta}_t}{\beta_t} + \beta_t \dot{\beta}_t \quad \forall t \in (0, 1),$$

which from Definition 4.1 is again equivalent to

$$\alpha_t^2 \frac{\dot{\beta}_t}{\beta_t} - 2\alpha_t \dot{\alpha}_t = \beta_t \dot{\beta}_t \quad \forall t \in (0, 1).$$

Denoting $a(t) := \alpha_t^2$ and observing that $\dot{a}(t) = 2\alpha_t \dot{\alpha}_t$ this is a first-order linear inhomogeneous ODE of the form

$$\dot{a}(t) - \frac{\dot{\beta}_t}{\beta_t} a(t) = -\beta_t \dot{\beta}_t.$$

Its solutions are of the form $a(t) = C\beta_t - \beta_t^2$. Imposing the boundary conditions $\alpha_1 = 0, \beta_1 = 1$ gives $C = 1$ so that $\alpha_t = \sqrt{\beta_t(1 - \beta_t)}$, or equivalently $\alpha_t^2 + \beta_t^2 = \beta_t$, as claimed.

Note that $\beta_t / \alpha_t = \sqrt{\beta_t} / \sqrt{1 - \beta_t} \rightarrow 0$ as $t \rightarrow 0_+$, or equivalently $\beta_t = o(\alpha_t)$ as $t \rightarrow 0_+$, as claimed. Similarly, $\alpha_t^2 / \beta_t = 1 - \beta_t \rightarrow 1$ as $t \rightarrow 0_+$ so that $\alpha_t^2 = O(\beta_t)$ as $t \rightarrow 0_+$. Differentiating yields

$$\dot{u}_t = \frac{d}{dt} \left(\frac{\beta_t}{\sqrt{\beta_t(1 - \beta_t)} + \beta_t} \right) = \frac{\dot{\beta}_t}{2\sqrt{\beta_t(1 - \beta_t)}(1 + 2\sqrt{\beta_t(1 - \beta_t)})} \rightarrow \lim_{t \rightarrow 0_+} \frac{\dot{\beta}_t}{2\sqrt{\beta_t}} \quad \text{as } t \rightarrow 0_+,$$

which proves that $\dot{u}_0 < \infty$ if and only if $\dot{\beta}_t = O(\sqrt{\beta_t})$ as $t \rightarrow 0_+$, as claimed. In that case we have shown that the schedule is indeed a point mass schedule as per Definition 6.1.

Finally, we prove the claimed identity for ε_t^* . We observe that $\dot{\alpha}_t = \dot{\beta}_t(1 - 2\beta_t)/(2\alpha_t)$ so that

$$\varepsilon_t^* = \alpha_t^2 \frac{\dot{\beta}_t}{\beta_t} - \alpha_t \dot{\alpha}_t = \dot{\beta}_t(1 - \beta_t) - \frac{1}{2} \dot{\beta}_t(1 - 2\beta_t) = \frac{1}{2} \dot{\beta}_t,$$

as claimed. It follows that also $\int_s^t 2\varepsilon_u^* du = \beta_t - \beta_s$ for any $0 \leq s \leq t \leq 1$. \square

Proposition 7.5 (linear velocity to lazy ODE velocity). *Define the schedule*

$$\alpha_t := (1 - t) / \sqrt{d_t}, \quad \beta_t := t / \sqrt{d_t}, \quad d_t := (1 - t)^2 + t^2,$$

as in Example 7.4 and assume we are given access to the ODE velocity $\bar{b} = v^{\text{flow}}$ of the linear interpolant from Definition 5.1. Then the velocity satisfies

$$b(t, x) = ((1 - 2t)/(d_t))x + (1/\sqrt{d_t})\bar{b}(t, \sqrt{d_t}x),$$

for all $(t, x) \in [0, 1] \times \mathbb{R}^d$. In particular, the initial velocity satisfies

$$b(0, z) = z + \bar{b}(0, z) = \mathbb{E}[X] \quad \forall z \in \mathbb{R}^d.$$

Proof. Observing that $c_t = 1/\sqrt{d_t}$, $\dot{c}_t = (1 - 2t)/(d_t\sqrt{d_t})$, $u_t = t$, $\dot{u}_t = 1$ and applying Proposition 5.4 with $\varepsilon \equiv 0$ so that also $\bar{\varepsilon} \equiv 0$ gives the conversion formula

$$b(t, x) = \frac{1 - 2t}{d_t}x + \frac{1}{\sqrt{d_t}}\bar{b}(t, \sqrt{d_t}x).$$

In particular, since $d_0 = 1$ and $u_0 = 0$ we get

$$b(0, z) = z + \bar{b}(0, z) = z + \mathbb{E}[X \mid Z = z] - \mathbb{E}[Z \mid Z = z] = \mathbb{E}[X].$$

Note that all equations are well-defined even when $t \in \{0, 1\}$. This concludes the proof. \square

Proposition 7.6 (linear velocity to lazy SDE drift). *Define the schedule*

$$\alpha_t := t(1 - t)/d_t, \quad \beta_t := t^2/d_t, \quad d_t := (1 - t)^2 + t^2,$$

as in Example 7.4 and assume we are given access to the ODE velocity $\bar{b} = v^{\text{flow}}$ of the linear interpolant from Definition 5.1. Then the statistically optimal SDE drift satisfies

$$b^*(t, x) = (2/d_t)((1 - 2t)x + t\bar{b}(t, (d_t/t)x)),$$

for all $(t, x) \in (0, 1] \times \mathbb{R}^d$, and the initial drift is identically zero, i.e. $b^*(0, 0) = 0$.

Proof. Observing that $c_t = t/d_t$, $\dot{c}_t = (1 - 2t^2)/d_t^2$, $u_t = t$, $\dot{u}_t = 1$ and applying Proposition 5.4 with $\varepsilon = \varepsilon^*$ so that

$$\bar{\varepsilon}_{u_t} = \bar{\varepsilon}_t = \frac{\alpha_t}{\beta_t} = \frac{1 - t}{t} = \bar{\varepsilon}_t^*$$

gives the conversion formula

$$b^*(t, x) = \frac{1 - 2t^2}{td_t}x + \frac{t}{d_t}\bar{b}^*\left(t, \frac{d_t}{t}x\right),$$

which is valid for $t \in (0, 1]$. With Proposition 4.2 we can convert the statistically optimal SDE drift $\varepsilon = \varepsilon^*$ to the ODE velocity ($\varepsilon \equiv 0$), which when applied to the linear interpolant evaluated in $(t, (d_t/t)x)$ reads

$$\bar{b}^*\left(t, \frac{d_t}{t}x\right) = 2\bar{b}\left(t, \frac{d_t}{t}x\right) - \frac{\dot{\beta}_t}{\beta_t} \frac{d_t}{t}x = 2\bar{b}\left(t, \frac{d_t}{t}x\right) - \frac{d_t}{t^2}x.$$

Inserting this into the expression for $b^*(t, x)$ gives

$$b^*(t, x) = \frac{1 - 2t^2 - d_t}{td_t}x + \frac{2t}{d_t}\bar{b}\left(t, \frac{d_t}{t}x\right) = \frac{2}{d_t}\left((1 - 2t)x + t\bar{b}\left(t, \frac{d_t}{t}x\right)\right),$$

which is still only valid for $t \in (0, 1]$. This proves the first part of the proposition. To analyze the case $t = 0$ we substitute $(t/d_t)x$ for x to get

$$b^*\left(t, \frac{t}{d_t}x\right) = \frac{2t}{d_t^2}(1 - 2t)x + \frac{2t}{d_t}\bar{b}(t, x) \rightarrow 0 \quad \text{as } t \rightarrow 0_+,$$

since $d_0 = 1$ and $\bar{b}(0, x) = \mathbb{E}[X] - x < \infty$ for all $x \in \mathbb{R}^d$. As also $(t/d_t)x \rightarrow 0$ as $t \rightarrow 0_+$ we see that the initial drift satisfies $b^*(0, 0) = 0$, as claimed. This concludes the proof. \square

B. Relationship to flows and diffusions

In this section we rigorously describe how the stochastic interpolant from Definition 1.1 relates to the objects studied in flow and diffusion models, respectively. The relationship to diffusion models is analyzed in section 5.1 in (Albergo et al., 2025) but to the best of our knowledge the particular connection to the statistically optimal diffusion scale ε^* (see Definition 4.1 and Theorem 4.3) as presented in Proposition B.5 has not been pointed out before.

First we prove some fundamental properties of the optimal diffusion scale ε^* .

Proposition B.1. *For any schedule (α, β) satisfying the criteria in Definition 1.1, ε^* from Definition 4.1 satisfies*

$$\begin{aligned}\varepsilon_0^* &:= \lim_{t \rightarrow 0_+} \varepsilon_t^* = \infty \quad \text{if } \lim_{t \rightarrow 0_+} \frac{\dot{\beta}_t}{\beta_t} \text{ exists,} \\ \varepsilon_t^* &\in (0, \infty) \quad \forall t \in (0, 1), \\ \varepsilon_1^* &= 0, \\ \int_0^t \varepsilon_s^* ds &= \infty \quad \forall t \in (0, 1].\end{aligned}$$

Proof. We have

$$\varepsilon_0^* := \lim_{t \rightarrow 0_+} \varepsilon_t^* = \lim_{t \rightarrow 0_+} \left(\alpha_t^2 \frac{\dot{\beta}_t}{\beta_t} - \alpha_t \dot{\alpha}_t \right) = \lim_{t \rightarrow 0_+} \frac{\dot{\beta}_t}{\beta_t} - \dot{\alpha}_0 = \lim_{t \rightarrow 0_+} \frac{d}{dt} \log(\beta_t) - \dot{\alpha}_0 = \infty,$$

if $\lim_{t \rightarrow 0_+} (\dot{\beta}_t / \beta_t)$ exists since $\alpha_0 = 1, |\dot{\alpha}_0| < \infty, \beta_0 = 0$ as well as $\beta_t > 0$ for $t > 0$. Strict positivity of ε^* for $t \in (0, 1)$ follows from the monotonicity assumptions $\dot{\alpha}_t < 0$ and $\dot{\beta}_t > 0$ for all $t \in (0, 1)$. $\varepsilon_1^* = 0$ follows from $\alpha_1 = 0, \beta_1 = 1, |\dot{\alpha}_1| < \infty, |\dot{\beta}_1| < \infty$.

To see that ε^* is not integrable, we use $\dot{\alpha}_t < 0$ for $t \in (0, 1)$ to bound $\varepsilon_t^* \geq \alpha_t^2 \frac{d}{dt} \log(\beta_t)$ and write

$$\int_0^t \varepsilon_u^* du = \lim_{s \rightarrow 0_+} \int_s^t \varepsilon_u^* du \geq \alpha_t^2 \lim_{s \rightarrow 0_+} \int_s^t \frac{d}{du} \log(\beta_u) du = \alpha_t^2 (\log(\beta_t) - \lim_{s \rightarrow 0_+} \log(\beta_s)) = \infty \quad \forall t \in (0, 1],$$

since $\beta_0 = 0$ and $\beta \in C^1([0, 1])$. This concludes the proof. \square

B.1. Flow models

In a flow model (or more precisely a *flow matching model*) one considers the time-dependent random variable $(1-t)Z + tX$ for $Z \sim \mathcal{N}(0, \mathbf{I})$ and $X \sim \rho_X$ independent with $t \in [0, 1]$. One then utilizes that the ODE

$$\frac{d}{dt} Y_t^{\text{flow}} = v^{\text{flow}}(t, Y_t^{\text{flow}})$$

with velocity field

$$v^{\text{flow}}(t, x) := \mathbb{E}[X \mid (1-t)Z + tX] - \mathbb{E}[Z \mid (1-t)Z + tX]$$

for $(t, x) \in [0, 1] \times \mathbb{R}^d$ generates ρ_X , i.e. $Y_1^{\text{flow}} \sim \rho_X$ whenever $Y_0^{\text{flow}} \sim \mathcal{N}(0, \mathbf{I})$. One sees that this corresponds exactly to the linear interpolant from Definition 5.1, i.e. $\bar{I}_t = (1-t)Z + tX$ and

$$\bar{b}(t, x) = \mathbb{E}[\dot{\bar{I}}_t \mid \bar{I}_t = x] = v^{\text{flow}}(t, x)$$

for all $(t, x) \in [0, 1] \times \mathbb{R}^d$, where we used the notation $\bar{b} := \bar{b}^{\bar{\varepsilon} \equiv 0}$ for the ODE velocity of the linear interpolant from Definition 5.1.

B.2. Diffusion models

In a variance-preserving diffusion model (or more precisely a *score-based generative model*) one corrupts data $\tilde{Y}_0 = X \sim \rho_X$ into noise $\tilde{Y}_\infty = Z \sim \mathcal{N}(0, \mathbf{I})$ through an Ornstein-Uhlenbeck process run from time 0 to ∞ (or some finite but large T in practice which introduces a bias),

$$d\tilde{Y}_s = -f(s)\tilde{Y}_s ds + g(s)d\tilde{W}_s,$$

with smooth and non-negative f, g satisfying

$$\int_0^\infty f(s) \, ds = \int_0^\infty g(s) \, ds = \infty,$$

so that the stationary distribution is indeed standard Gaussian, i.e. $\tilde{Y}_\infty \sim \mathcal{N}(0, \mathbf{I})$.

One then uses Anderson's time reversal (Anderson, 1982) to construct the unique reverse-time process run from ∞ (or T) to 0 that turns noise into data with the same joint distribution as the forward process. This reverse-time process depends on the score function of the Ornstein-Uhlenbeck process with initial distribution ρ_X .

To compare diffusion models to flow models and stochastic interpolants one must compactify time via some C^1 monotonically increasing bijection $\phi : [0, \infty) \rightarrow [0, 1]$ satisfying $\phi(0) = 0$ and $\lim_{s \rightarrow \infty} \phi(s) = 1$, with inverse $\psi := \phi^{-1} : [0, 1] \rightarrow [0, \infty)$. One can then define $Y_\tau := \tilde{Y}_{\psi(\tau)}$ for $\tau \in [0, 1]$, and by a limiting argument extend to $\tau \in [0, 1]$. Using similar standard stochastic calculus techniques as in the proof of Theorem 5.5 one gets that

$$dY_\tau = -f(\psi(\tau))\psi'(\tau) Y_\tau \, d\tau + g(\psi(\tau))\sqrt{\psi'(\tau)} \, dW_\tau,$$

with

$$W_\tau := \int_0^{\psi(\tau)} \sqrt{\phi'(s)} \, d\tilde{W}_s.$$

In particular, if we take $\phi(s) = 1 - \exp(-s)$ so that $\psi(\tau) = -\log(1 - \tau)$ and $\psi'(\tau) = 1/(1 - \tau)$, we get the Ornstein-Uhlenbeck process

$$dY_\tau = -\frac{f(-\log(1 - \tau))}{1 - \tau} Y_\tau \, d\tau + \frac{g(-\log(1 - \tau))}{\sqrt{1 - \tau}} \, dW_\tau.$$

As the following Proposition B.5 shows, when one chooses the statistically optimal diffusion scale $\varepsilon = \varepsilon^*$ in the stochastic interpolant framework, the corresponding reverse-time SDE becomes an Ornstein-Uhlenbeck process in the time range $[0, 1]$. Before stating this result we need to introduce the *backward drift* as in (Albergo et al., 2025) as well as the core result analogous to Theorem 1.4 along with an intra-interpolant conversion result similar to Proposition 4.2.

Definition B.2 (backward drift). For an interpolant as in Definition 1.1 and $\varepsilon : [0, 1] \rightarrow [0, \infty], \varepsilon \in C^1((0, 1])$ we define the backward drift

$$\overset{\leftarrow}{b}{}^\varepsilon(t, x) := \dot{\alpha}_t \eta_Z(t, x) + \dot{\beta}_t \eta_X(t, x) - \varepsilon_t s(t, x).$$

We refer the reader to Albergo et al. (2025) for a proof of the following result.

Theorem B.3. Define $\tau := 1 - t$ and $\overset{\leftarrow}{W}_\tau := -W_\tau = -W_{1-t}$. Then the solutions to the family of reverse-time SDEs

$$d\overset{\leftarrow}{X}_\tau^\varepsilon = -\overset{\leftarrow}{b}{}^\varepsilon(\tau, \overset{\leftarrow}{X}_\tau^\varepsilon) \, d\tau + \sqrt{2\varepsilon_\tau} \, d\overset{\leftarrow}{W}_\tau,$$

solved forward in reverse-time τ with $\overset{\leftarrow}{X}_0^\varepsilon \sim \rho_X$ independent of $\overset{\leftarrow}{W}$, satisfy $\text{Law}(\overset{\leftarrow}{X}_\tau^\varepsilon) = \text{Law}(I_{1-\tau})$ for all $\tau \in [0, 1]$.

The following proposition can be proved analogously to Proposition 4.2.

Proposition B.4. For a fixed interpolation schedule (α, β) and $\varepsilon : [0, 1] \rightarrow [0, \infty)$, the backward drift from Definition B.2 can be expressed in terms of the score through the equation

$$\overset{\leftarrow}{b}{}^\varepsilon(t, x) = (\varepsilon_t^* - \varepsilon_t) s(t, x) + \frac{\dot{\beta}_t}{\beta_t} x,$$

for all $(t, x) \in (0, 1) \times \mathbb{R}^d$.

We now state and prove our own result.

Proposition B.5. *Let $\overset{\leftarrow}{b}^* := \overset{\leftarrow}{b}^{\varepsilon^*}$ be the statistically optimal (in forward-time) reverse-time drift for any (non point mass) stochastic interpolant as per Definition 1.1. Then the associated reverse-time SDE from Theorem B.3 is a time-scaled Ornstein-Uhlenbeck process of the form*

$$d\overset{\leftarrow}{X}_\tau^* = -\frac{\dot{\beta}_\tau}{\beta_\tau} \overset{\leftarrow}{X}_\tau^* d\tau + \sqrt{2\varepsilon_\tau^*} d\overset{\leftarrow}{W}_\tau,$$

solved forward in reverse time τ with initial condition $\overset{\leftarrow}{X}_0^* \sim \rho_X$. If additionally the interpolant is variance-preserving, i.e. $\alpha_t^2 + \beta_t^2 = 1$ for all $t \in [0, 1]$, then the reverse-time SDE reduces to

$$d\overset{\leftarrow}{X}_\tau^* = -\varepsilon_\tau^* \overset{\leftarrow}{X}_\tau^* d\tau + \sqrt{2\varepsilon_\tau^*} d\overset{\leftarrow}{W}_\tau.$$

Proof. The SDE from Theorem B.3 reads

$$d\overset{\leftarrow}{X}_\tau^\varepsilon = -\overset{\leftarrow}{b}^\varepsilon(\tau, \overset{\leftarrow}{X}_\tau^\varepsilon) d\tau + \sqrt{2\varepsilon_\tau} d\overset{\leftarrow}{W}_\tau.$$

Using Proposition B.4 with $\varepsilon = \varepsilon^*$ gives

$$\overset{\leftarrow}{b}^*(\tau, x) = \frac{\dot{\beta}_\tau}{\beta_\tau} x,$$

so that the SDE from Theorem B.3 reduces to

$$d\overset{\leftarrow}{X}_\tau^* = -\frac{\dot{\beta}_\tau}{\beta_\tau} \overset{\leftarrow}{X}_\tau^* d\tau + \sqrt{2\varepsilon_\tau^*} d\overset{\leftarrow}{W}_\tau,$$

as claimed. Assuming now that $\alpha_\tau^2 + \beta_\tau^2 = 1$, i.e. assuming that the schedule is variance-preserving, gives

$$\varepsilon_\tau^* = (1 - \beta_\tau^2) \frac{\dot{\beta}_\tau}{\beta_\tau} - \alpha_\tau \left(\frac{-\dot{\beta}_\tau \beta_\tau}{\alpha_\tau} \right) = \frac{\dot{\beta}_\tau}{\beta_\tau},$$

so that the SDE from Theorem B.3 reduces to

$$d\overset{\leftarrow}{X}_\tau^* = -\varepsilon_\tau^* \overset{\leftarrow}{X}_\tau^* d\tau + \sqrt{2\varepsilon_\tau^*} d\overset{\leftarrow}{W}_\tau,$$

as claimed. □

C. Schedule visualizations

The first row of Figure 4 visualizes the linear schedule (see Definition 5.1) used in flow matching models alongside the lazy ODE and SDE schedule, respectively (see Proposition 7.1 and in particular Example 7.4). The second row visualizes the statistically optimal diffusion scale ε^* (see Definition 4.1 and Theorem 4.3) associated with each schedule. The figure uses the denominator definition $d_t := (1 - t)^2 + t^2$. Note that these are the schedules and diffusion scales used in Figure 1.

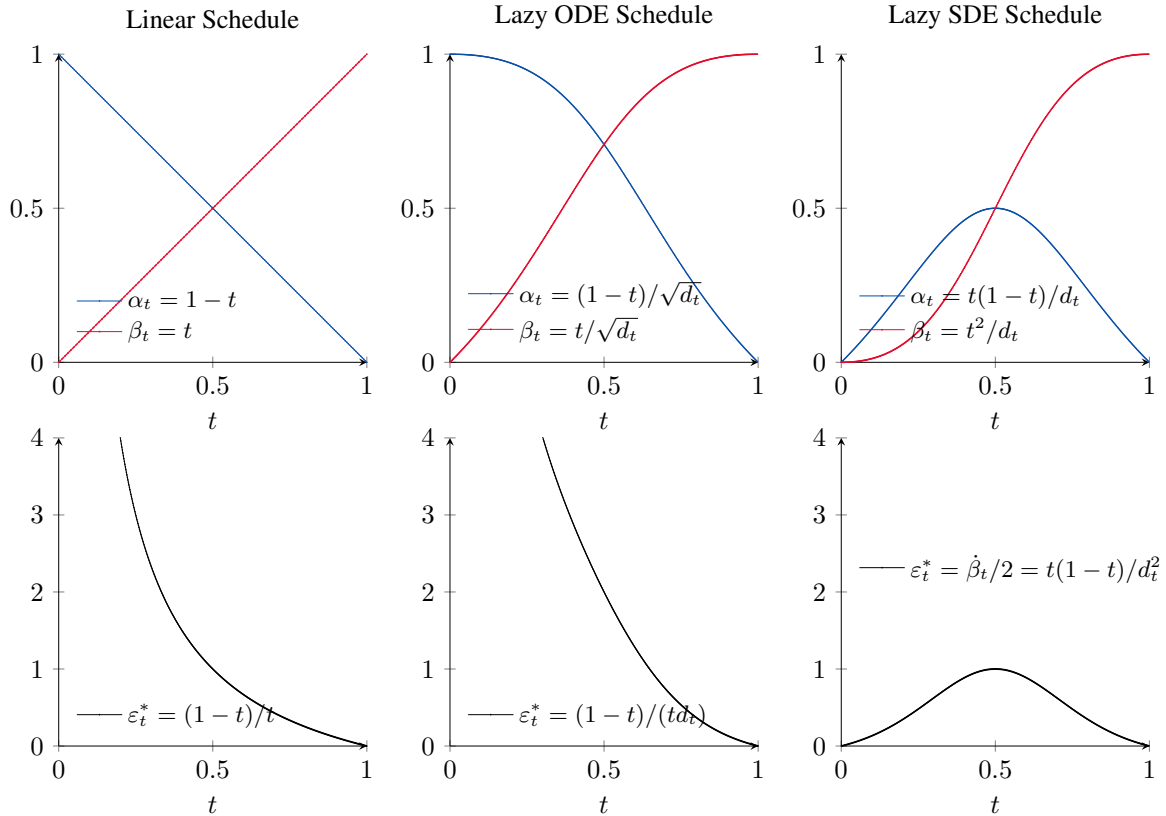


Figure 4. Schedules (α, β) (top row) and corresponding statistically optimal diffusion scale ε^* (bottom row). These are the schedules and diffusion scales used in Figure 1.

D. Pseudocode for lazy ODE and SDE sampling

Algorithms 1 and 2 give pseudocode for the algorithmic formulation of Propositions 7.5 and 7.6 using the explicit Euler and Euler-Maruyama solver, respectively. We stress that any ODE or SDE solver can be used in practice.

Algorithm 1 ODE-Sample

Input: linear velocity \bar{b} , step size Δt

$t \leftarrow 0$
 $x \leftarrow \text{sample } \mathcal{N}(0, I)$
while $t < 1$ **do**

$d \leftarrow 1 + 2t(t - 1)$

$$b \leftarrow \frac{1-2t}{d} x + \frac{1}{\sqrt{d}} \bar{b}(t, \sqrt{d} x)$$

$$x \leftarrow x + \Delta t b \\ t \leftarrow t + \Delta t$$

end while

Return: x

(explicit Euler step)

Algorithm 2 SDE-Sample

Input: linear velocity \bar{b} , step size Δt

$$d_{\text{next}} \leftarrow 1 + 2\Delta t(\Delta t - 1)$$

$$\beta_{\text{next}} \leftarrow \left(\frac{\Delta t}{d_{\text{next}}} \right)^2$$

$$\Delta W \leftarrow \text{sample } \mathcal{N}(0, \beta_{\text{next}} \mathbf{I})$$

$$t \leftarrow \Delta t$$

$$x \leftarrow \Delta W$$

$$(X_0^* = b^*(0, 0) = 0)$$

while $t < 1$ **do**

$$d \leftarrow d_{\text{next}}$$

$$\beta \leftarrow \beta_{\text{next}}$$

$$b^* \leftarrow \frac{2}{d} \left((1 - 2t)x + t \bar{b}(t, \frac{d}{t} x) \right)$$

$$t_{\text{next}} \leftarrow t + \Delta t$$

$$d_{\text{next}} \leftarrow 1 + 2t_{\text{next}}(t_{\text{next}} - 1)$$

$$\beta_{\text{next}} \leftarrow \left(\frac{t_{\text{next}}}{d_{\text{next}}} \right)^2$$

$$\Delta W \leftarrow \text{sample } \mathcal{N}(0, (\beta_{\text{next}} - \beta) \mathbf{I})$$

$$x \leftarrow x + \Delta t b^* + \Delta W$$

$$t \leftarrow t + \Delta t$$

end while

Return: x

(Euler-Maruyama step)

E. ODE and SDE numerical integration schemes

Below we give numerical schemes for solving the SDE from Theorem 1.4 with drift b^ε and additive diffusion scale ε ,

$$dX_t^\varepsilon = b^\varepsilon(t, X_t^\varepsilon) dt + \sqrt{2\varepsilon_t} dW_t.$$

With $\varepsilon \equiv 0$ the SDE degenerates to an ODE and e.g. the Euler-Maruyama scheme becomes the explicit Euler scheme. Note that the experiments either use $\varepsilon \equiv 0$ or $\varepsilon = \varepsilon^*$, and with the schedules we consider the quadratic variation from time s to t ($0 \leq s \leq t \leq 1$) under the latter diffusion scale, $\int_s^t 2\varepsilon_u^* du$, can be calculated analytically (see Proposition 7.1 and Proposition 5.2) and is therefore used in the below schemes and in our experiments.

For a total of $N > 1$ solver steps we use a fixed step size of $\Delta t = \frac{1}{N}$. We denote the solution after $n \in \{0, 1, \dots, N\}$ steps by Y_n at time $t_n = n\Delta t$. For $n < N$ the independent Wiener process increments from time t_n to t_{n+1} are denoted $\Delta W_n \sim \mathcal{N}(0, \Delta t \mathbf{I})$ and we define $V_n := \left(\int_{t_n}^{t_{n+1}} 2\varepsilon_t dt \right) \Delta W_n / \Delta t$. With the “corrected” solution at time n denoted by \tilde{Y}_n and initially defined as $\tilde{Y}_0 := Y_0$ the update step from Y_n to Y_{n+1} is then defined as below.

Euler-Maruyama

$$Y_{n+1} = Y_n + \Delta t b^\varepsilon(t_n, Y_n) + V_n.$$

Predictor-Corrector

$$\begin{aligned} Y_{n+1} &= \tilde{Y}_n + \Delta t b^\varepsilon(t_n, Y_n) + V_n, \\ \tilde{Y}_{n+1} &= \tilde{Y}_n + \frac{1}{2} \Delta t (b^\varepsilon(t_n, Y_n) + b^\varepsilon(t_{n+1}, Y_{n+1})) + V_n. \end{aligned}$$

Heun

$$\begin{aligned} Y_{n+1} &= \tilde{Y}_n + \Delta t b^\varepsilon(t_n, \tilde{Y}_n) + V_n, \\ \tilde{Y}_{n+1} &= \tilde{Y}_n + \frac{1}{2} \Delta t (b^\varepsilon(t_n, Y_n) + b^\varepsilon(t_{n+1}, Y_{n+1})) + V_n. \end{aligned}$$

We use a variant of the predictor-corrector and Heun scheme in which the final, returned solution is Y_N so that the corrected final solution \tilde{Y}_N is never computed. This prevents us from ever having to evaluate the drift b^ε at $t = 1$.⁸

Note that the “correct” step for the predictor-corrector scheme is equivalent to the Heun scheme. They both use an Euler-Maruyama “predict” step and only differ in whether the drift in this step is evaluated in Y_n or \tilde{Y}_n . This detail means that the Heun scheme uses two drift evaluations per step while the Euler-Maruyama and predictor-corrector schemes only use one. Since evaluating this drift function in practice amounts to doing an expensive forward pass in a neural network the Heun scheme is therefore roughly twice as slow as it requires $2N - 1$ function evaluations instead of N . To compare the three schemes fairly, we used half the amount of steps for the Heun scheme compared to the predictor-corrector and Euler-Maruyama schemes.

For the PRX model and settings used in our experiments we find that the predictor-corrector scheme generally converges faster as a function of drift evaluations than the Euler-Maruyama and Heun scheme, especially for SDE generation. This is indicated by Figure 5 and Figure 6 which consider sample images generated with the standard linear flow model schedule using the ODE generation ($\varepsilon \equiv 0$) and statistically optimal SDE generation ($\varepsilon = \varepsilon^*$), respectively, for the same prompt “Two husky’s hanging out of the car windows”. One sees that the predictor-corrector scheme converges to the reference image at 4096 steps (at which the Heun scheme has used 2048 steps) slightly faster than the Euler-Maruyama and Heun scheme. All schemes more or less converge to the same reference image, as expected.

Note that the choice of integration scheme is not important for our experiments since the purpose is not to investigate which scheme leads to better image generation (faster convergence) but rather to assess the effect of transforming to the lazy schedule whilst keeping the integration scheme fixed.

⁸Evaluating the drift at $t = 1$ is in fact not a problem for us. The PRX flow model we use uses linear ODE velocity parameterization and no division by zero (which can potentially occur since $\alpha_1 = 0$) is introduced in our conversion formulas from this linear velocity to the ODE velocities and SDE drifts we consider.

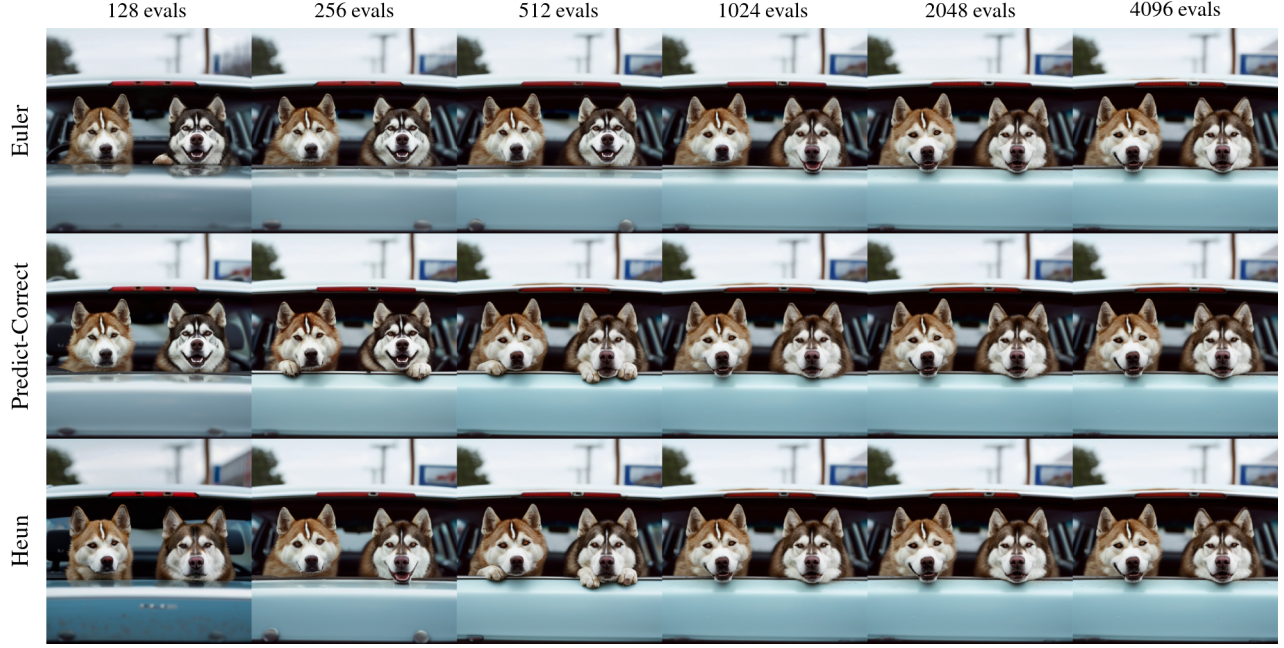


Figure 5. Sample images from the PRX flow model with varying number of steps using different integration schemes for the ODE with original linear flow model schedule. A guidance strength of 5 with the text prompt “Two husky’s hanging out of the car windows” was used.

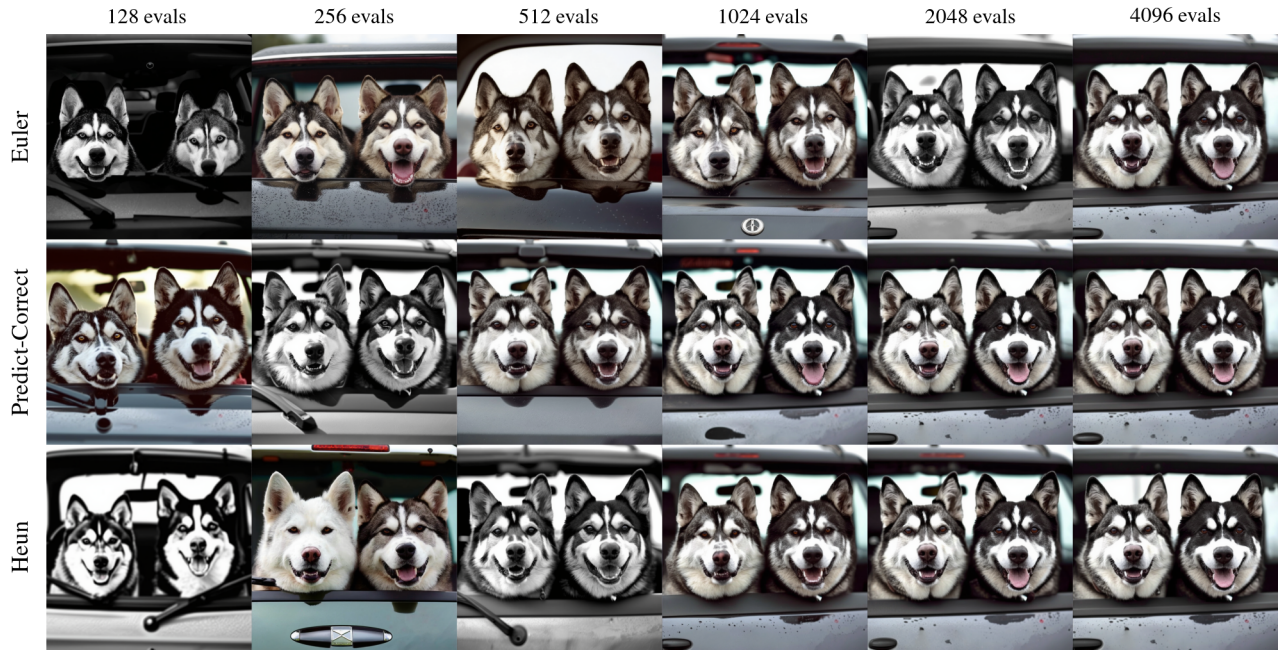


Figure 6. Same as Figure 5 but for the statistically optimal SDE with original linear flow model schedule.

F. Further experimental results

F.1. Solver convergence animations

The solver convergence is better visualized as an animation than as a static image. Figure 7 shows sample images for 5 prompts generated with 64 predictor-corrector solver steps. An animation over multiple solver steps is available at [this Zenodo link](#). Heuristically, we find that after 64 steps the SDE solutions are comparable to the ODE solutions in fidelity, but this is of course a subjective matter.

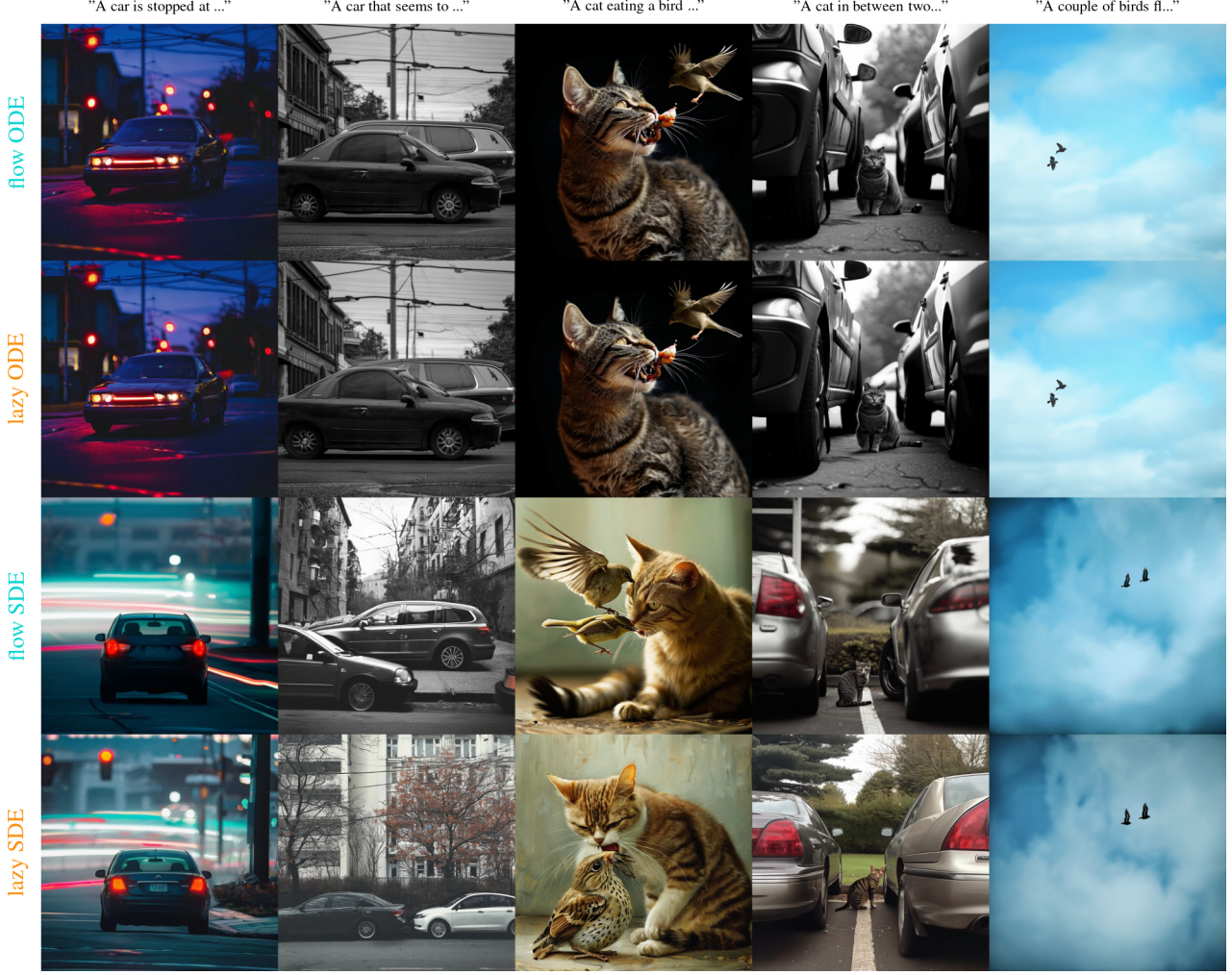


Figure 7. Sample images generated using 64 predictor-corrector steps for 5 different prompts from our experiment. Each row corresponds to whether an ODE or SDE is used and whether the original linear `flow` model schedule or the conversion to the `lazy` schedule is used. An animation over all solver step amounts $\{4, 8, \dots, 4096\}$ is available at [this Zenodo link](#).

F.2. Equivalence of convergence

Here we test whether the ODE and SDE solutions converge to the same reference image irrespectively of whether the flow or lazy schedule is used. For each n_i amount of solver steps we calculate the RMSE between the image generated with the original linear flow model schedule against the image generated with the conversion to the lazy one using n_i steps, i.e. we calculate

$$\text{RMSE}(\text{img}_{n_i}^{\text{ODE,flow}}, \text{img}_{n_i}^{\text{ODE,lazy}})$$

for each i and similarly for the SDE. We then average over all 100 prompts and plot this average as a function of n_i for the ODE and SDE, respectively. The result is shown in Figure 8. The figure indicates that both the ODE and SDE converge to

the same reference image irrespectively of which schedule is used, but this convergence is much faster for the ODE than for the SDE. This is probably due to the fact that the flow and lazy schedule are somewhat similar for ODE generation (in particular they both satisfy $\alpha_0 = 1$), while for SDE generation the lazy schedule is a point mass schedule (see Figure 4). Since the flow model velocity is not learned perfectly, approximation errors make the flow-to-lazy schedule transform inexact which amplifies more for SDE generation relative to ODE generation.

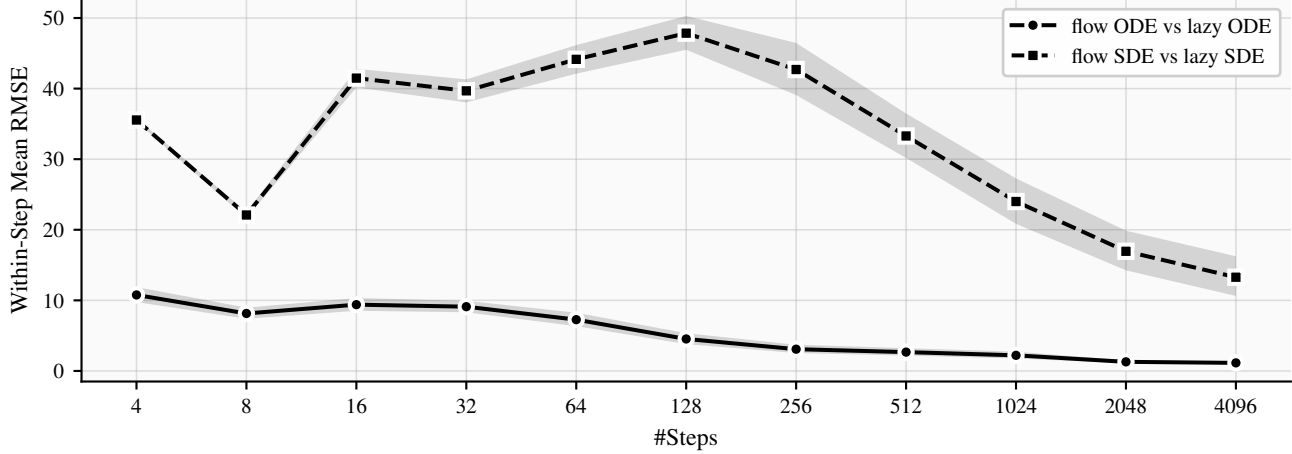


Figure 8. Within-step mean RMSE as a function of the number of solver steps using the predictor-corrector scheme. By “within-step RMSE” we mean the RMSE between the image generated under the original linear flow model schedule versus that generated using the conversion to the lazy schedule for a fixed number of solver steps, for the ODE and SDE, respectively. Shaded area indicates a 95% confidence interval calculated by bootstrapping with 10,000 samples. The plot indicates that the RMSE converges to zero as the number of solver steps grows, as one would expect, although the convergence is much faster for the ODE than for the SDE.

F.3. Convergence results using the flow image as a common reference

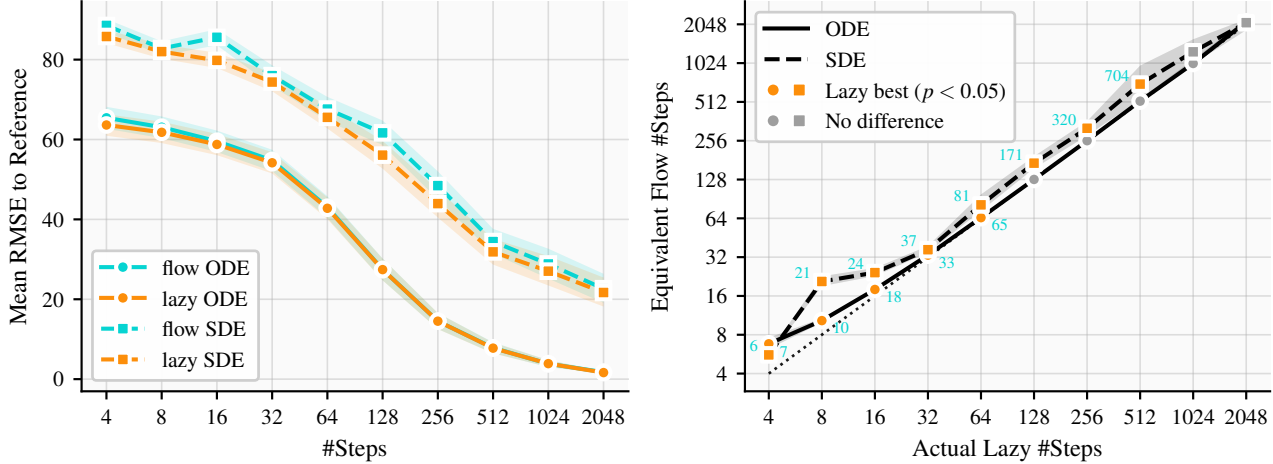


Figure 9. Same as Figure 3 but with $\text{img}_{\text{reference}}^{\text{ODE}} := \text{img}_{4096}^{\text{ODE,flow}}$ instead of $\text{img}_{\text{reference}}^{\text{ODE}} := (\text{img}_{4096}^{\text{ODE,flow}} + \text{img}_{4096}^{\text{ODE,lazy}})/2$, and similarly for the SDE.

Here we recreate Figure 3 but instead of defining

$$\text{img}_{\text{reference}}^{\text{ODE}} := (\text{img}_{4096}^{\text{ODE,flow}} + \text{img}_{4096}^{\text{ODE,lazy}})/2,$$

we instead define

$$\text{img}_{\text{reference}}^{\text{ODE}} := \text{img}_{4096}^{\text{ODE,flow}},$$

and similarly for the SDE. Clearly this puts the lazy schedule method at a disadvantage. However, Figure 9 shows that even with this disadvantage the lazy schedule converges statistically significantly faster most of the time. As one would

expect, the results are slightly worse, e.g. the lazy schedule is not statistically significantly better for SDE generation at 1024 solver steps compared to the linear flow schedule, whereas when using the average reference as common reference it is (see Figure 3).

G. COCO captions

The COCO validation dataset consists of images with five human generated captions each. We extract the first caption from the first 100 images and remove any potential trailing period. We use the resulting 100 sentences as text prompts for the PRX flow model. These are shown below sorted alphabetically (ASCII-wise).

- 1 A bathroom sink with toiletries on the counter
- 2 A bathroom with a poster of an ugly face above the toilette
- 3 A bathroom with a sink and shower curtain with a map print
- 4 A bathroom with a toilet, sink, and shower
- 5 A bathroom with a traditional toilet next to a floor toilet
- 6 A beautiful dessert waiting to be shared by two people
- 7 A bicycle replica with a clock as the front wheel
- 8 A bike leaning against a sign in Scotland
- 9 A black Honda motorcycle parked in front of a garage
- 10 A black and white photo of an older man skiing
- 11 A black and white toilet with a plunger
- 12 A black cat is inside a white toilet
- 13 A boat that looks like a car moves through the water
- 14 A brown and black horse in the middle of the city eating grass
- 15 A brown purse is sitting on a green bench
- 16 A car is stopped at a red light
- 17 A car that seems to be parked illegally behind a legally parked car
- 18 A cat eating a bird it has caught
- 19 A cat in between two cars in a parking lot
- 20 A couple of birds fly through a blue cloudy sky
- 21 A cute kitten is sitting in a dish on a table
- 22 A delivery truck with an advertisement for Entourage
- 23 A dirt bike rider doing a stunt jump in the air
- 24 A dog and a goat with their noses touching at fence
- 25 A dog sitting between its masters feet on a footstool watching tv
- 26 A door with a sticker of a cat door on it
- 27 A dual sink vanity with mirrors above the sinks
- 28 A few items sit on top of a toilet in a bathroom stall
- 29 A fighter jet is flying at a fast speed
- 30 A fireplace with a fire built in it
- 31 A gas stove next to a stainless steel kitchen sink and countertop
- 32 A green car on display next to a busy street
- 33 A group of people preparing food in a kitchen
- 34 A group of people riding mopeds in a busy street
- 35 A kitchen is shown with wooden cabinets and a wooden ceiling
- 36 A large U.S Air Force plain sits on an asphalt ramp
- 37 A large passenger airplane flying through the air
- 38 A large passenger jet taking off from an airport
- 39 A little girl in a public bathroom for kids
- 40 A long empty, minimal modern skylit home kitchen
- 41 A man getting a drink from a water fountain that is a toilet
- 42 A man in a wheelchair and another sitting on a bench that is overlooking the water
- 43 A man is sitting on a bench next to a bike
- 44 A man sits with a traditionally decorated cow
- 45 A man standing in a kitchen while closing a cupboard door
- 46 A parade of motorcycles is going through a group of tall trees
- 47 A person holding a skateboard overlooks a dead field of crops
- 48 A person walking in the rain on the sidewalk

49 A photograph of a kitchen inside a house
 50 A picture advertising Arizona tourism in an airport
 51 A picture of a man playing a violin in a kitchen
 52 A pinewood and green modern themed kitchen area
 53 A public bathroom with a bunch of urinals
 54 A random plane in the sky flying alone
 55 A room with blue walls and a white sink and door
 56 A shot of an elderly man inside a kitchen
 57 A small car is parked in front of a scooter
 58 A small child climbs atop a large motorcycle
 59 A small closed toilet in a cramped space
 60 A tiny bathroom with only a toilet and a shelf
 61 A toilet sits next to a window and in front of a shower
 62 A trio of dogs sitting in their owner's lap in a red convertible
 63 A variety of pots are stored in a nook by a fireplace
 64 A woman is walking a dog in the city
 65 An airplane with its landing wheels out landing
 66 An all white kitchen with an electric stovetop
 67 An office cubicle with four different types of computers
 68 An office cubicle with multiple computers in it
 69 An old toilet with a hello kitty cover top
 70 An old-fashioned green station wagon is parked on a shady driveway
 71 Fog is in the air at an intersection with several traffic lights
 72 Half of a white cake with coconuts on top
 73 Jet liner flying off into the distance on an overcast day
 74 Little birds sitting on the shoulder of a giraffe
 75 Man in motorcycle leathers standing in front of a group of bikes
 76 Office space with office equipment on desk top
 77 Pedestrians walking down a sidewalk next to a small street
 78 People are waiting for the bus near a bus stop
 79 Posted signs point the way through a parking garage
 80 Riding a motorcycle down a street that has no one else on it
 81 Rows of motor bikes and helmets in a city
 82 Several motorcycles riding down the road in formation
 83 The airplane is on the runway with two young men standing by
 84 The back door with a window in the kitchen
 85 The sign of a restaurant in the outside of the store
 86 The telephone has a banana where the receiver should be
 87 The woman in the kitchen is holding a huge pan
 88 The young man is stirring his pot of food with a wooden spoon
 89 This is an open box containing four cucumbers
 90 Two husky's hanging out of the car windows
 91 Two women waiting at a bench next to a street
 92 Women father around a desk and machinery in a factory
 93 a bike leaning on a metal fence next to some flowing water
 94 a counter with vegetables, knife and cutting board on it
 95 a man sleeping with his cat next to him
 96 a man with a bike at a marina
 97 a modern flush toilet in a bathroom with tile
 98 a small toilet stall with a toilet brush and 3 rolls of toilet paper
 99 an airport with one plane flying away and the other sitting on the runway
 100 four urinals in a public restroom with a window